International Journal of Precision Engineering and Manufacturing (2024) 25:453–485
https://doi.org/10.1007/s12541-023-00870-z

Online ISSN 2005-4602
Print ISSN 2234-7593

REVIEW

# Advanced Surface Engineering Approaches for Exotic Applications

**Sutanuka Mohanty[1] · Soumyabrata Basak[2,4] · Debasis Saran[1] · Kajari Chatterjee[1] · Turin Datta[3] · Atul Kumar[1] · Chandra Prakash[1] · Doo-Man Chun[2] · Sung-Tae Hong[2] · Kisor Kumar Sahu[1]**

Received: 1 February 2023 / Revised: 30 July 2023 / Accepted: 31 July 2023 / Published online: 9 August 2023


**Abstract**
Selection and classification of suitable materials for exotic applications, including aviation/space, nuclear, oil &gas industries, are still challenging since these applications are typically very demanding in terms of microstructural, mechanical, and electrochemical properties. Surface engineering plays an important role in controlling the properties of the exposed surface, which play key roles in interfacing with another material or exposure to the environment, promoting desirable chemical reactions, and suppression of corrosion. Hence, modification of the surface characteristics of desired materials to the desired depth without altering their bulk properties is essential. The present review focuses on using some of the latest and most advanced surface engineering tool sets such as laser, electron beam (EB), friction stir processing (FSP), ion beam, and plasma immersion ion implantation (PIII). Such techniques provide substantial improvements in wear and corrosion resistance, reduction in frictional losses, increased fatigue life, and enhanced chemical stability at high temperatures for exotic applications.

**Keywords** Surface engineering · Laser · Electron beam · Friction stir processing · Ion beam · Plasma immersion ion implantation

## 1 Introduction

The aviation and global space industries have been projected to grow rapidly in the coming decades. For instance, a recent study by Morgan Stanley suggests that the global space industry has been projected to create a revenue of $1 trillion by 2040 [1]. Similarly, in the next two decades, the aerospace sector is estimated to grow at a compounded annual rate of 4.3% [2]. In addition, demand for petroleum products, clean electricity and a booming world economy will positively contribute to old economy sectors such as oil & gas and nuclear industries [3, 4]. According to an International Atomic Energy Agency report, the global nuclear-generating capacity will increase from the current level of 392 GW (2019) to 715 GW by 2050 [5]. Undoubtedly, these demand-related developments will come with both significant challenges and growth opportunities for exotic applications in aviation, oil & gas, nuclear, and space industries. Furthermore, the operating environment for these sectors is harsh and requires constant improvements in materials selections, design and development of components, robust safety standards compliance, surface modification for enhanced performance, low wear and high corrosion resistance, etc. As a perspective, corrosion and related surface engineering challenges alone have led to a loss of roughly 3.4% of the world's GDP in 2013, according to a National Association of Corrosion Engineers (NACE) study [6].

The material surface has intrinsically higher free energy when compared with the bulk, which facilitates the initiation and progression of physicochemical

Sutanuka Mohanty and Soumyabrata Basak are co-first authors.

This paper is an invited paper (Invited Review)

✉ Sung-Tae Hong
sthong@ulsan.ac.kr

✉ Kisor Kumar Sahu
kisorsahu@iitbbs.ac.in

[1] School of Minerals, Metallurgical and Materials Engineering, Indian Institute of Technology Bhubaneswar, Bhubaneswar 752050, India

[2] School of Mechanical Engineering, University of Ulsan, Ulsan 44610, Republic of Korea

[3] School of Nanoscience and Technology, Indian Institute of Technology Kharagpur, Kharagpur, West Bengal 721302, India

[4] School of Engineering and Technology, Adamas University, Kolkata, West Bengal 700126, India

processes such as catalysis, adsorption, adhesion, and diffusion from the surface [7]. Apart from the physicochemical processes, the failure of any material in service due to environmental degradation also initiates from a surface [8]. Components involved in the structural and functional parts of these exotic industries undergo severe degradation due to wear, corrosion, oxidation, fatigue, hydrogen embrittlement, and erosion caused by their challenging working environment, like extreme radiation and temperature, severe weather, saltwater exposure, etc. [10–14]. This leads to failure of the components that cause catastrophic accidents resulting in loss of time, production cost, and most importantly, loss of human lives and other living beings [9–14]. Traditional metals and alloys, which are generally developed for applications in benign conditions, typically struggle to meet the performance requirements for extreme exotic conditions. Some widely used surface treatment methods for improving the surface properties are energy beam processes (laser, electron, and ion beam), plasma immersion ion implantation (PIII), friction stir processing (FSP), nitriding, carburizing, coatings, shot peening, rolling, and many more. These surface treatment technologies are mainly classified into conventional and advanced techniques, as mentioned in Fig. 1.

Out of these, applications of advanced surface engineering approaches (laser, electron and ion beam, PIII, and FSP) often can turn out to be a more economically feasible solution than designing a completely new material for such specialized purposes. These techniques modify the microstructure and/or composition, thus altering the chemistry, mechanical and tribological properties of the near-surface region of a component to improve surface-dependent engineering properties [9]. They also have some major advantages, for example, high precision, uniform distribution of energy, shorter processing time, and lower energy consumption. This paper will cover only the advanced surface engineering techniques that have a high potential for use in the previously mentioned exotic applications.

## 2 Surface Engineering Challenges in Exotic Applications

Various types of surface challenges are faced by the materials/components used in exotic applications because of their continuous exposure to harsh and unforgiving working conditions like high doses of radiation and temperature, high pressure, and corrosive environments. This section provides a summary of various challenges faced by the materials/components used in these exotic applications.

### 2.1 Nuclear

This section starts with some popular structural materials used in the nuclear industry. The challenges faced are discussed as are research targeted at addressing them. Some important candidate materials include but are not limited to, 316L stainless steel, Duplex stainless steel (DSS), Inconel alloys like Alloy 690 and Alloy 625, Austenitic A709, and Hastelloy C-276. These materials possess very good mechanical properties like high hardness, strength, fatigue, and ductility. They also have exceptionally good tribological properties and enhanced corrosion resistance. When these materials are exposed to the harsh environments of reactors receiving a high dosage of nuclear radiation, deterioration of the tribological properties is usually observed, and these materials face surface-related problems like irradiation-induced hardening/segregation, swelling of the surface, and phase transition. Other environmental degradation processes commonly observed in nuclear power plants include intergranular stress corrosion cracking (IGSCC), irradiation-assisted stress corrosion cracking (IASCC), and the release of metal ions from the surface. Material degradation in a nuclear power plant is a phenomenon involving various aspects of materials, environment, and stress states, which progressively reduces the performance of the components used in the nuclear industry, causing sudden failure [15]. Figure 2 shows different stress corrosion cracking (SCC) phenomena in light water reactor (LWR) power plants,

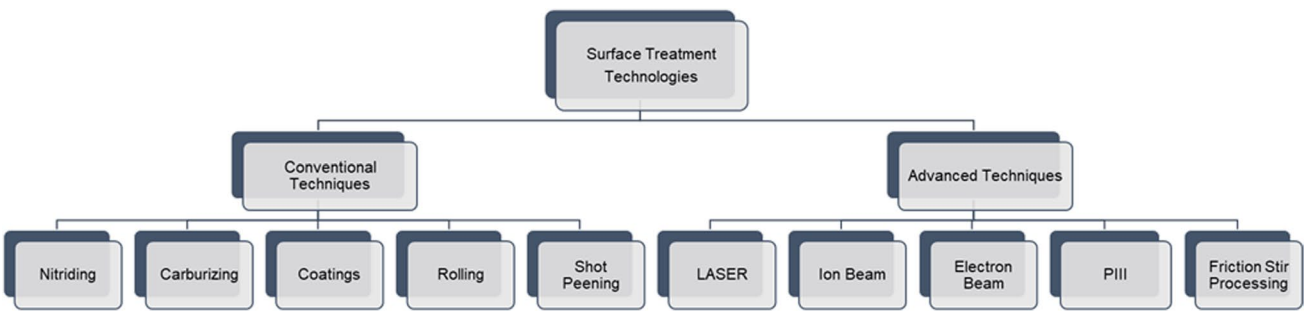


**Fig. 1** Classification of various surface treatment technologies

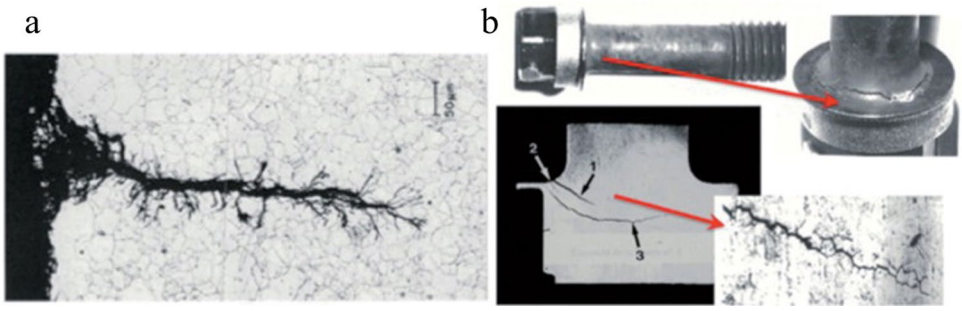


**Fig. 2** **a** Primary water SCC in steam generator tubing in LWR power plants and **b** irradiation-assisted SCC in a pressurized water reactor baffle bolts. Reproduced with permission from [15]

which reveal complex materials degradation in the nuclear industry.

Uranium is the most common fuel used to power commercial nuclear reactors that produce electricity. It is also used to produce isotopes for medical and industrial usage. Uranium metal is highly reactive and pyrophoric, and it is oxidized easily in hot and humid environments, which has detrimental effects for both future storage and disposal [16]. Additionally, zirconium alloys (Zr alloys) are utilized as important structural materials for water-cooled nuclear reactors. Zr alloys such as Zr-1Nb, Zr-2.5Nb are widely used for cladding/protection tubes for nuclear fuel rods (i.e., pellets of uranium dioxide or other fissionable materials that power a nuclear reaction). Zr-alloys are typically used in nuclear plants due to their low neutron (produced during fission reaction) absorption cross-section, high-in-service heat and chemical corrosion resistance, adequate high-temperature mechanical properties and dimensional stability in the presence of radiation [17–19]. However, the major concern in the use of Zr-alloys is its interaction with hydrogen. During service under irradiation flux, Zr-alloys are exposed to elevated temperature and high-pressure cooling water, which releases hydrogen by water hydrolysis or by oxidation of Zr fuel claddings under the "loss of coolant accident" (LOCA) conditions. The absorption of hydrogen leads to the precipitation of hydrides in the alloy. The mechanical integrity of the cladding undergoes embrittlement due to the presence of brittle hydrides [17, 18]. Zirconium alloy claddings act against the release of fission products into the coolant, providing mechanical integrity to the cladding, which is of utmost importance in nuclear plants and forms the first line of defense against any nuclear disaster.

## 2.2 Offshore Oil and Gas

Oil and gas are key sources of primary energy for human progress. They are also used as essential ingredients for other engineering materials such as plastics, paints, chemicals, and much more. Oil and natural gas are most often found in large quantities at the bottoms of seas, lakes, and swamps formed over hundreds of millions of years from dead organic materials. Giant platforms and sophisticated drilling techniques are presently used to extract crude oil and gas from the immense depths of the ocean.

Valves, pipes, and pumps used in the oil & gas industry are mostly made from austenitic stainless steel (ASS), high-strength low-alloy steel (HSLA), DSS, and Inconel alloys. These are employed for subsea extraction and transportation of oil and gas because of their high strength, toughness, ductility, and, most importantly, high corrosion resistance in corrosive environments [20]. Offshore oil and gas environments contain highly reactive chemical species like chloride, bromide, and iodide salts, hydrogen sulfide ($H_2S$), $CO_2$, and organic acids [21, 22]. The presence of these deleterious species in oil and gas wells poses surface-related problems to the material like galvanic and crevice corrosion, sulfide stress corrosion cracking (SSC), IGSCC, and hydrogen embrittlement (HE) (Fig. 3). IGSCC and HE are reviewed below in Sects. 3.1.4 and 3.2.3.2, respectively.

Erosion of the materials from the surface due to the flow of fluids also leads to the problem of crevice corrosion. Chloride ions in seawater, liquefied natural gas, sand and other abrasive substances carried by the fluid in pipelines, along with the presence of defects due to poor surface finish, reduce the lifespan of the equipment. This further aggravates leaks and other problems by inducing wear and corrosion. In addition, the high extraction pressure also accelerates the breakdown of the components used in these extraction processes [6, 7]. Bacterial activity inside the pipeline increases the toxicity of the flowing fluids by producing waste products like $H_2S$, $CO_2$, and organic acids, causing corrosion inside the pipeline [21].

## 2.3 Aviation and Space

Since the first artificial earth satellite in 1957, the space industry has progressively emerged as one of the most rapidly expanding and lucrative industries. The data obtained from the satellites improve our life on earth by offering many applications, starting from precise navigation, land/forest/sea surveillance to environmental tracking of the earth [23]. The progress in this sector has resulted in extraordinary achievements such as the moon landing, exploration of other planets (such as Mars and Venus), celestial bodies (moon, comet,

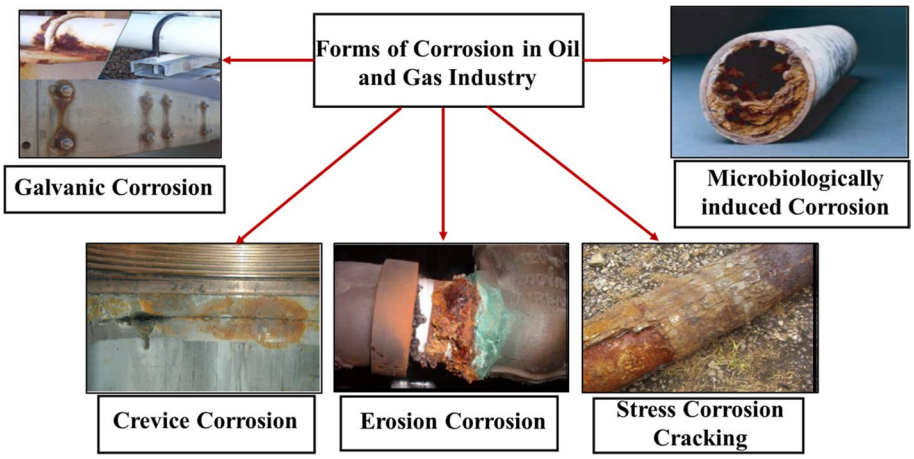


**Fig. 3** Different types of corrosion in the oil & gas industry. Open source: https://prog.lmu.edu.ng/colleges_CMS/document/books/CHE431%20%20Types%20of%20corrosion%20in%20Oil%20and%20Gas%20Industry%20.pdf)

asteroids) and the development of the international space station, which creates new opportunities for researchers to extend the frontiers of knowledge. Other than space exploration, the aviation industry is also a key contributor to the global economy by connecting different continents, countries, and cultures, benefiting the entire human race.

The structural and engine components used in spacecraft and aircraft are generally made of metal alloys and polymer-based composites, which suffer from cyclic loads during take-off, flight, and landing [24–26]. This causes fatigue cracking, stress corrosion cracking, and fretting wear in the components. The bearings used in the main shafts of aircraft and spacecraft typically carry heavy loads and are very important for prolonging their life during their operation in unforgiving conditions. Under such harsh conditions, the bearing suffers failure due to contact fatigue, wear, corrosion, plastic deformation, and fracture, which lead to premature failure of space and aircraft engines [27]. Al-based alloys (AA) are extensively used in the aviation and space industry. For example, AA2024 is used in the seat ejectors of commercial airplanes, and AA7075 is used for wing skins, fuselage skins, panels and covers. Apart from that, Mg-based alloys are currently used in Boeing 737 s and 747 s. However, Mg-alloys are highly susceptible to corrosion, and pose a serious challenge for its usage in the outer shells of the aircraft [28]. Accelerated erosion is another serious concern for long-life satellites and space stations orbiting in low earth orbit (LEO; 200–2000 km above the earth's surface). At this altitude, the materials suffer degradation due to the attack of highly reactive atomic oxygen (AO), high energy vacuum ultraviolet (UV) radiation emitted from the sun, extreme temperature conditions (175 to 160 °C), ionizing radiation and collision impacts from space debris [29–33]. AO is mainly responsible for the degradation of spacecraft materials. Kapton® is a preferred material used on the surfaces of spacecraft in LEO because of its resistance to UV radiation and thermal stability ranging from – 269 to 400 °C. Prolonged exposure of Kapton® to LEO results in degradation of material as depicted in Fig. 4b and c.

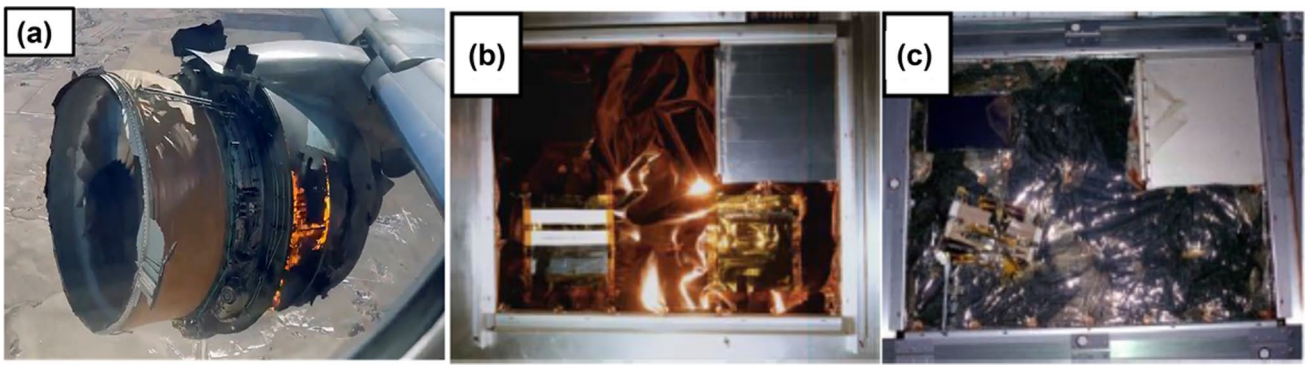


**Fig. 4** **a** Engine failure in Boeing 777 triggered by metal fatigue; Kapton® **b** before and **c** after six years exposure to LEO. Reproduced with permission from [33]

## 3 Advanced Approaches in Surface Engineering for Exotic Applications

### 3.1 Laser

The use of laser as a source of heat is a non-equilibrium processing technique for surface modification of materials that deposits large amounts of energy in an alloy over a short time and can spatially be limited near the surface [34]. Laser processing is typically characterized by an exponential energy deposition profile with controlled energy (1–30 J/cm$^2$) and power ($10^4$–$10^7$ W/cm$^2$) inputs either in the form of short pulses ($10^{-3}$–$10^{-12}$ s) or continuous waves [35, 36]. The main advantages of laser lie in the formation of its very rapid heating and cooling rate ($10^4$–$10^{11}$ K/s), extremely high thermal gradient ($10^6$–$10^8$ K/m) and ultra-rapid re-solidification velocity (1–30 m/s) that can significantly alter the microstructure and composition in the near-surface region without affecting the bulk properties [36]. As our focus in this paper lies in the improvement of only surface properties of structural materials for exotic applications, we have briefly reviewed two techniques, i.e., laser surface melting and laser surface texturing, which require minimal energy for altering the near-surface region without any phase transformation in the surface and bulk. Unlike laser alloying and cladding, which alters the microstructure and composition in near-surface regions, laser surface melting and laser surface texturing alter only the microstructure without changing the composition.

#### 3.1.1 Laser Surface Melting (LSM)

Laser surface melting (LSM) is one of the most popular laser-based surface modification techniques whereby the surface of the material is locally melted using high-power continuous waves [37–40]. Popular laser sources include Nd: YAG and $CO_2$ lasers [41]. After localized surface melting, microstructural modifications are usually observed on the melted surface due to rapid re-solidification [42–46]. Such local interactions (melting and re-solidification) occur over a very short time interval, which significantly improves the mechanical properties of the near-surface region. A schematic representation of the process of LSM is shown in Fig. 5. The entire surface can be scanned to produce overlapping parallel tracks for modification of the larger area of the substrate. Typically, the important process parameters of LSM are wavelength, laser power, scan speed and shielding gas pressure.

A continuous-wave $CO_2$ laser has been used for improving the hardness and wear resistance of Hastelloy C-276 with LSM process parameters: 2 mm spot diameter, 0.6 MPa argon gas pressure, process power between 1.25 kW to 1.75 kW, and scan speed of 300 mm/min [47]. In another investigation by Cui [48], the depth of the metal pool of AZ31B Mg alloy processed by LSM increased with an increase in laser power, which is schematically represented in Fig. 6. Charee and Tangwarodomnukun [49] also observed deeper case depth (210 µm) in AISI 9254 high silicon spring steel when processed using higher laser power (10 W) and a slower scan speed (5 mm/s) as compared with other processing conditions (laser power 4 W, 6 W, 8 W and scan speeds of 10 mm/s and 15 mm/s).

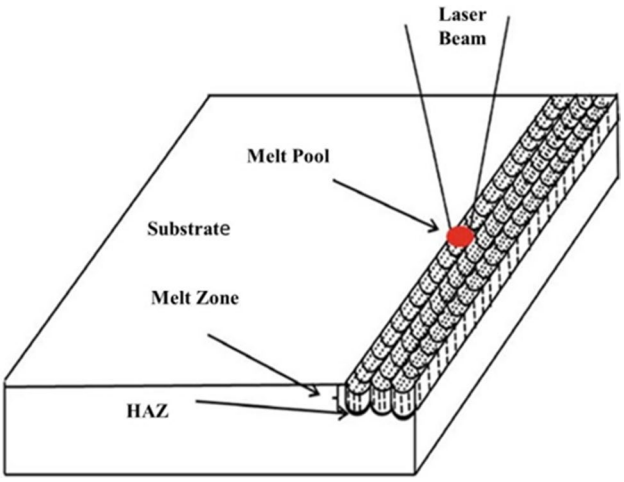


**Fig. 5** Schematic representation of laser surface melting. Reproduced with permission from [41]

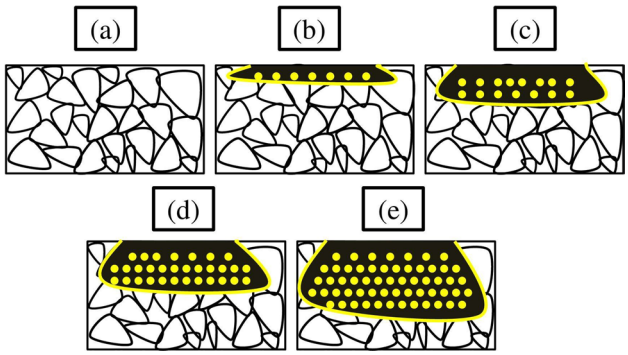


**Fig. 6** Schematic representation of **a** microstructure of AZ31B Mg-alloy substrate showing the grain structure. Schematic microstructural representation of the depth of the laser melted zone for the laser power of **b** 1600 W, **c** 1800 W, **d** 2000 W, and **e** 2200 W [48]

#### 3.1.2 Laser Surface Texturing (LST)

LST uses high-power single-mode pulsed lasers, which ablate the surface of a material and produce a desired texture

or patterns on the surface [50–55]. Typically, the patterns that are formed on the surface after LST can be dimples, grooves, and free forms [50, 56]. LST works on the principle of the laser ablation process, where focused beam irradiation on the surface leads to the melting and vaporization of the irradiated zone [57, 58]. Local heating of the irradiated zone removes material and subsequently changes the texture, creating micro-patterns on the surface, which is schematically represented in Fig. 7.

LST can also be accomplished by two other approaches, i.e., (a) laser interference and (b) laser shock peening. In the laser interference technique to obtain LST, the periodic patterns are obtained by interference of the coherent laser beams [59–65]. Local melting of the surface is observed due to maximum interference, which corresponds to the highest laser intensity [66]. With this technique, some patterns like lines, dots, and cross-like patterns can be produced on the surface. This technique has recently gained significant momentum in electronics and semiconductor device fabrication for data storage and integrated circuits, optical telecommunications, and photonic crystal science [67]. In-situ laser interference patterning has been used for the epitaxial growth of precise InAs quantum dots on nano-island GaAs (100) surfaces [68].

Laser shock peening (LSP) is a very recent and advanced technique that induces shock waves and generates texture based on plastic deformation without introducing any thermal event [69–75]. This technique can improve the tribological properties of engineering materials as it induces compressive residual stress and improves hardness on the surface [60, 71–78].

For LST, the laser parameters that must be precisely controlled for successfully obtaining the desired surface morphology and feature sizes are laser power intensity, laser spot size, and pulse repetition frequency [32]. For ablation and interference-based LST, the laser power determines the overall morphology of the texture feature and the area of the heat-affected zone [69]. The amount of plastic deformation in LSP depends on the shockwave pressure, which is largely controlled by the laser power intensity [69, 79–82].

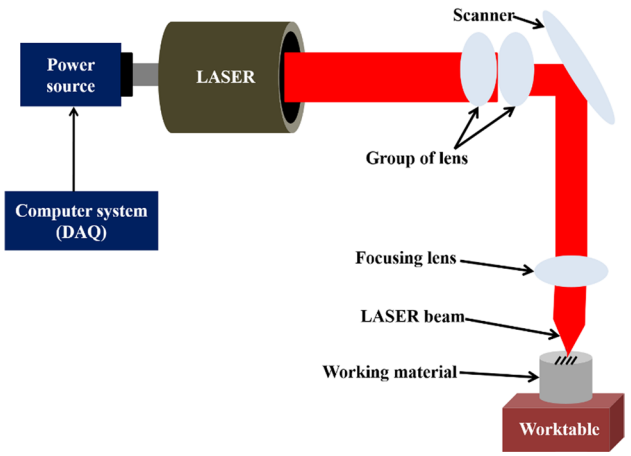


**Fig. 7** Schematic representation of laser surface texturing. Reproduced with permission from [60]

The laser pulse duration can be distinguished for millisecond, nano-second, pico-second and femto-second lasers [83–85]. Bathe et al. [86] studied the effect of laser pulse duration on grey cast iron processed using ablation-based LST. Their investigation revealed an improved coefficient of friction (CoF) when processed using a millisecond laser (~0.31) as compared to a nanosecond laser (~0.02) and a femtosecond laser (~0.01). Figure 8 reveals the textured surface morphologies of the cast iron obtained using scanning electron microscopy (SEM).

The dimple formed like a bulge due to the ejection of the molten material and deposition on it after processing by a millisecond laser (Fig. 8b). However, as compared with the surface obtained after processing by the millisecond and nanosecond laser, the smoothest surface characterized by sharper dimple profile was obtained using a femtosecond laser (Figs. 8e and f).

Apart from the laser power and pulse duration, the number of pulses can control the size, depth, and shape of the surface texturing [60]. Yang et al. [87] found the mean radii of the textured surface increased from 12.72 µm to 13.37 µm when the number of pulses increased from 10 to 90 in aluminum AA 2024-T3 alloy at the same laser power intensity.

### 3.1.3 LSM in Nuclear and Oil & Gas Industries

316L ASS, which is widely used in the nuclear industry, is susceptible to phase transition due to radiation-induced segregation, misorientation of the grain boundaries (SGBs), and changes in the lattice parameter. Lin et al. [88] reported that when 80 keV Ar ions with a fluence of $2.96 \times 10^{15}$ ions/cm$^2$ (3.7 dpa) at room temperature were irradiated on the cold-rolled 316L, the phase transition from γ (FCC) → α′ (BCC) was observed, which led to an increase in the lattice parameter from 3.5989 Å to 3.6005 Å after irradiation. After treating the surface with LSM, it was observed that 316L ASS maintains its austenite phase (which was stable after LSM treatment), making the material surface immune to radiation. ASS and DSS (e.g., 304SS and UNS 32750) are very susceptible to sensitization, where the carbides of chromium form along the grain boundaries of the material. The chromium-depleted regions result in the formation of less stable passive layers, which ultimately causes IGSCC in these alloys [89, 90]. LSM is an effective processing technique to eliminate sensitization in aged ASSs (UNS S30400, S31603, S32100, and S34700) and aged DSSs (UNS S31803 and S32950) [90]. The degree of sensitization (DOS) of the alloys ranged from 15.6% to 36.6% before LSM and reduced

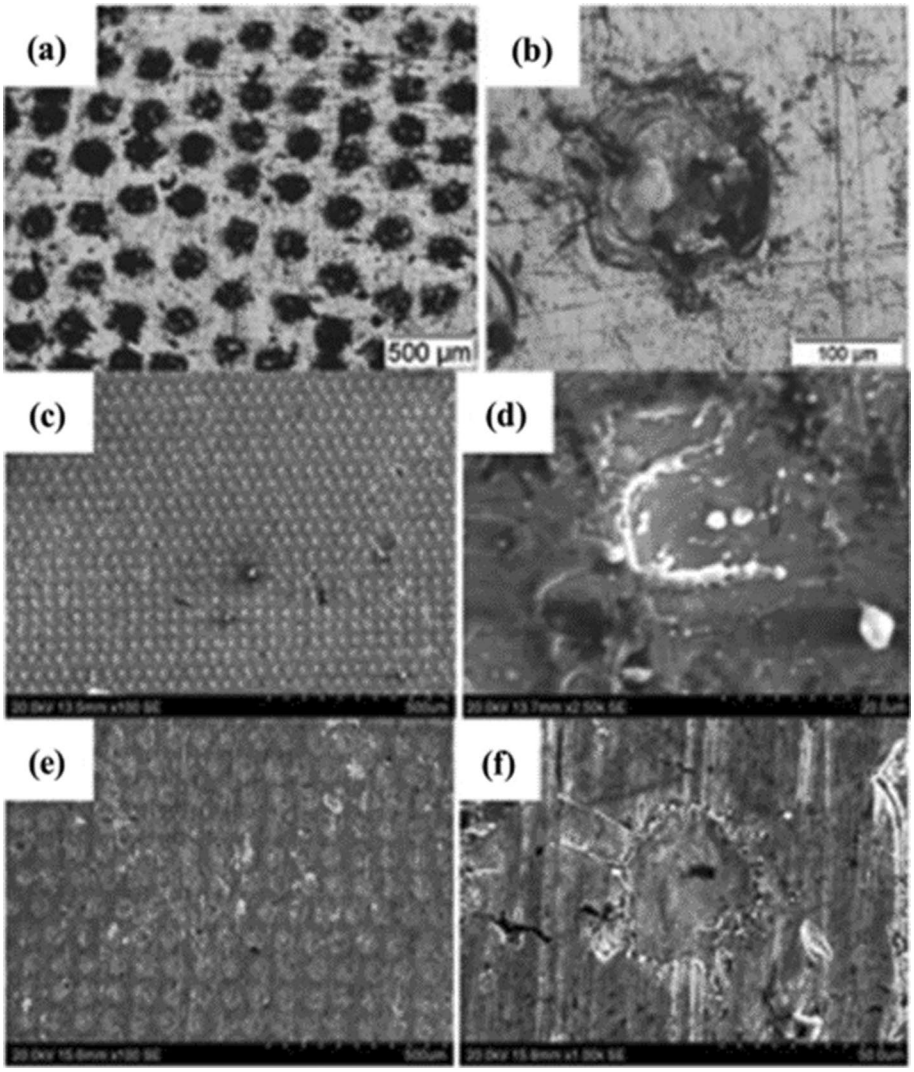


**Fig. 8** Surface morphology of grey cast iron obtained after ablation-based LST using **a** millisecond laser (0.5 ms), **c** nanosecond laser (40 ns), and **e** femtosecond laser (120 fs). The individual dimples are magnified and shown for each pulse duration in (**b**), (**d**) and (**f**). Reproduced with permission from [60]

in the range varying from 1.2% to 1.46% after LSM. This was due to the dissolution of carbides (or sigma phase), which reduced Cr-depleted regions in the microstructure and enhanced the intergranular corrosion resistance of the aged alloys, as shown in Fig. 9 [90].

A study by Lim et al. [91] shows the value of DOS was reduced from 16.5 to 3.42% after LSM on Inconel 600, which is used for making steam generator tubing material in nuclear power plants. Suh and co-workers observed the mode of fracture as brittle intergranular in sensitized alloys, whereas the fracture mode was ductile trans-granular after LSM [41]. Pacquentin et al. [92] carried out LSM treatment on the surface of Alloy 690 (~ laser density of 3.6 J/cm$^2$, 70% overlap) and observed a continuous layer of $Cr_2O_3$ formed on the surface of an alloy having a thickness of 8 nm. It was also noted that the rate of release of Ni ions from Alloy 690 was reduced by seven times in the heating phase of the generator and 3.7 times in the overall process, which is a significant improvement over the conventional surface. Hashim et al. [93] studied the effect of LSM on Hastelloy C-276 (used in nuclear and petrochemical industries) and reported that the surface hardness of LSM treated Hastelloy C-276 increased by roughly 60%. They found that the wear resistance of the LSM treated specimen also increased by approximately four times.

Tang et al. [94] reported an improvement in the cavitation erosion resistance by LSM in manganese-nickel-aluminum-bronze (MAB) alloys, which are generally used in marine propellers. The cavitation erosion resistance was significantly improved (by 5.8 times) as compared to that of as-received MAB due to the formation of a homogeneous and refined microstructure as well as improvement in hardness after LSM treatment. Cottam et al. [95] investigated the cavitation erosion resistance in nickel-aluminum-bronze (NAB) with LSM and observed that the weight loss was 0.002 g after the cavitation erosion test for 4 h, which was approximately 13 times lower than the as-received NAB sample. Kwok et al. [96] reported significant improvement

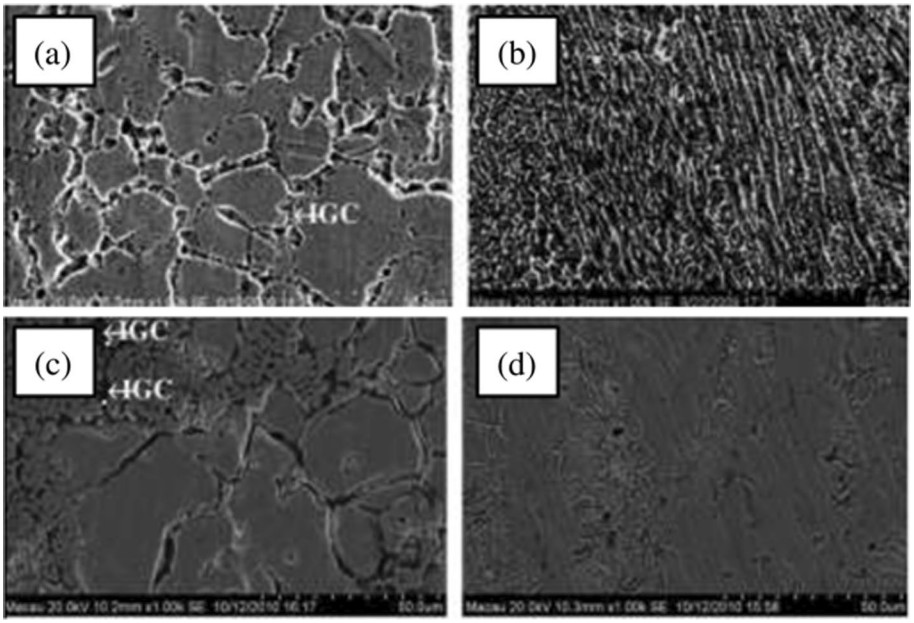


**Fig. 9** Corrosion morphologies after double-loop electrochemical potentio-kinetic reactivation (DL-EPR) test for **a** aged S31603 ASS before LSM, **b** aged S31603 ASS after LSM, **c** aged S31803 DSS before LSM and **d** aged S31803 DSS after LSM. Reproduced with permission from [90]

in cavitation erosion resistance in LSM treated UNS S42000 martensitic stainless steel, which was nearly 70 times lower than that of as-received and annealed specimens and 1.8 times lower than that of heat-treated specimens.

#### 3.1.4 LSM in Aviation and Space Industries

Mg alloys are favorable materials for making components in the aerospace industry mostly because of their high strength-to-weight ratio. Cast Mg alloys generally consist of coarse microstructures having grain sizes in the range of 50–250 µm. LSM treatment of Mg alloys resulted in a significant reduction in grain sizes (1–10 µm) due to the rapid solidification rate, which favors grain refinement as well as the formation of dendritic networks. Grain refinement results in an increase in surface hardness of approximately two to four times as compared to cast alloy [97].

Abbas et al. [98, 99] reported that improvement in wear resistance of AZ31 and AZ61 Mg alloy was noted due to the formation of intermetallic β-$Mg_{17}Al_{12}$ during LSM, which hindered the propagation of micro-cracks and increased the resistance to plastic deformation during wear. Dutta Majumdar et al. [100] reported improvement in the corrosion resistance of Mg alloys after LSM treatment due to significant grain refinement and redistribution of the precipitates along the grain boundaries. Selective evaporation of Mg alloys during LSM resulted in enrichment of Al, Zn and Ce on the surface, which resists further corrosion of the Mg alloys. Mondal et al. [101] observed the corrosion resistance of ACM720 Mg alloys after LSM treatment and reported that there was a slight improvement in corrosion due to the formation of the continuous layer of $Mg(OH)_2$ on the treated surface. Dissolution of the $Al_2Ca$ phase and enrichment of Al on the surface also enhanced the corrosion resistance.

Ti alloys usually have low hardness, low wear resistance and a higher CoF, which restricts its usage in some applications due to fretting wear and reduced fatigue life [102]. When the surface of Ti was treated with LSM, a fine layer of martensite formed, which increased the surface hardness and also showed excellent wear and corrosion resistance due to the formation of a thin film of $TiO_2$ [102]. Langlade et al. [103] reported that by varying the laser treatment parameters, titanium layers of TiO, $TiO_2$ and $TiO_3$ formed, which significantly improved the corrosion resistance. It was also reported that the pitting potential of the Ti alloy increased from 3.51 to 5.56 V after LSM treatment [104].

Although the tribological properties of Al alloys are significantly improved when the surface was treated with LSM, there are some difficulties associated with LSM. For example, it's high oxidation potential and surface reflectivity lead to low energy absorption, which enhances the formation of microstructural defects like porosities and crack formation. Rodríguez et al. [105] reported that when the surface of a 6061 Al alloy substrate (used in the fuel tank of aircraft) was reinforced with Al-multi walled carbon nanotubes (Al-MWCNTs) and treated with LSM, the surface hardness was increased up to 43% when compared to the 6061- aluminum alloy substrate. In contrast, the LSM of pure aluminum increased the hardness by about 28%. The presence of Al-MWCNT powder also increased the energy absorption of the laser, which resulted in deeper modification of the surface.

#### 3.1.5 LST in Aviation and Oil & Gas Industries

A case study by Gadiv Petrochemical Industries Ltd. revealed that the lifespan of LST mechanical seals (used in pumps) increased significantly [106]. It was noticed that the laser textured seal operated for more than 10,000 h over a period of 38 months, whereas the non-textured seal was replaced four times during the same period. Texture density, which is defined as the ratio of textured surface area to the total surface area, is a critical parameter for determining the tribological properties of a surface. Optimal texture density reduces the CoF and increases the wear resistance of the surface. Li et al. [107] investigated the effect of texture feature density on the tribological behavior of AISI 52100 bearing steels (used to manufacture aircraft bearings). They observed that improvement in wear resistance was noted by texturing the surface through laser interference, and the highest wear resistance was obtained at 15% texture density. Sasi et al. [108] reported the effect of LST on the HSS tool for machining AA7075-T6 aerospace alloys. In this study, the authors made uniform circular-shaped dimples on the surface of the tool. The use of textured tools reduced the cutting force up to 9% and the thrust force by 19% (operating at 30 m/s).

LST produces a hydrophobic surface, which provides excellent corrosion resistance due to its anti-biofouling property. Hydrophobicity can be readily achieved by creating a periodic, 3D micro and nano-patterned topography on the surface of the material. In most cases, it was observed that the surface turned from hydrophilic to hydrophobic after the LST when exposed to airborne organic contaminants (fluoroalkyl silanes, silicone sol, and other surface modifiers) for a longer period of time [109]. In addition, studies revealed that the corrosion resistance of the surface was enhanced in marine water due to anti-biofouling and superhydrophobicity [110].

In recent years, picosecond laser texturing (PLT) has been used for creating various types of textures on the surface of titanium, stainless steel, copper, and aluminum alloys, which are mostly used in nuclear, aviation, and oil & gas industries. Yang et al. [111] developed a super-hydrophobic/super-hydrophilic (SH/SHL) surface via PLT and chemical modification to control drop splashing on AA7075 alloys. It was observed that after PLT, the surface was initially super-hydrophilic. It became hydrophobic after immersion in ethanol and stearic acid for 60 min, followed by exposure to organic contaminants, which ultimately improved the corrosion resistance of the surface. Sun et al. [112] investigated the role of PLT on AISI 304 ASS and chemically modified the surface with silicon-sol after the PLT treatment. Thus, hydrophobicity was achieved, which resulted in a surface with anti-biofouling properties. Super-hydrophobic surfaces possessing micro-groove arrays and micro pits reduced the mean microbe attachment area ratio (MAAR) from 92 to 57% [112].

CrMnFeCoNi is a high entropy alloy (HEA) and is widely used in both nuclear and aviation industries due to its superior mechanical properties like high strength, ductility at cryogenic temperature, superior fatigue life and tribological properties. Tong et al. [113] studied the LSP process on CrMnFeCoNi HEA with laser parameters (wavelength 1064 nm, pulse width 10 ns, working frequency 5 Hz, spot diameter 3 mm, and overlap rate 70% with different laser energies of 2 J, 4 J, and 6 J). The authors found that the highest surface roughness (Ra = 1.61 µm) and compressive residual stress (131 MPa) were obtained with a laser energy input of 6 J. A challenge in the space industry is increasing the efficiency of solar panels that are used in satellites. The main factor that improves efficiency is reducing the reflectivity of light from the solar panel, and the reflectivity of the light could be lowered by texturing the surface of the solar panel, as shown in Fig. 10 [114]. Horn et al. [115] reported that the reflectivity of the surface could be reduced to 11% using a laser influence of 4 J/cm$^2$ when compared to the standard multi-crystalline Si solar cell textured surface.

Increasing the joining strength of Ti–6Al–4V alloy (TC4) and carbon fiber reinforced thermoplastic composites (CFRTPs), i.e., CFRTP/TC4, is challenging due to the low shear strength between the joints [116]. Caiwang et al. [117] reported laser joining of CFRTP/TC4 by inducing a texture depth of 100 µm by LST on a Ti alloy. The shear strength of the joined material was 2618 N, which was approximately 156% higher than the un-textured alloy. Ge et al. [118] reported that LSP treatment of AZ31 Mg alloy increased the fatigue life of the material due to a reduction in the rate of crack length with respect to the number of cycles. The primary cause for the decrease in crack length

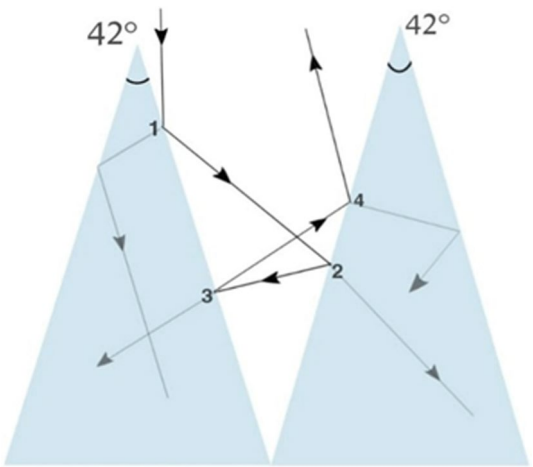


**Fig. 10** Path traced by optical light incident on laser-textured silicon surfaces. Reproduced with permission from [114]

was the presence of fine grains and compressive residual stress, which increased the number of grain boundaries that acted as a barrier for crack propagation and small planar slip distance. The grain size before LSP was 16.4 μm, and it was 17.5 nm after LSP.

## 3.2 Ion Beam

Ion beam technique offers a sensitive, rapid, and non-destructive tool for altering properties (e.g., structural, physicochemical and interface properties) in a controlled manner. It consists of charged particle ions (mainly, gallium or argon), typically generated from a liquid metal ion source (LMIS) in the presence of a strong electric field. This is also a valuable technique to estimate the engineered material properties up to a superficial depth. Ion beam technology is widely used in electronics, manufacturing, nuclear, aviation and space industries. The process mechanism of the ion beam techniques is schematically represented in Fig. 11.

### 3.2.1 Ion Beam Processing

Ion beam processing provides new avenues of sample characterization and analysis and the ability to develop smart materials by modifying their properties. There are three major aspects in the ion beam processing of materials: the science behind ion beam irradiation, material selection, and surface engineering (schematically shown in Fig. 12) [119]. These can be fairly addressed in terms of the commonly available ion beam analysis techniques and the task-specific modification using ion beams.

#### 3.2.1.1 Modification of Materials by Ion Beam

(i) *Ion beam mixing* In this technique, mixing of interfaces, highly adherent coated layers, or growing layers is accomplished by recoiled ion collisions with target atoms. Ion beam mixing improves various properties at the target interface by inter-diffusivity [120], relieving stresses [121], and the formation of advanced alloy layers [122]. These modifications depend on the mass of the incident ion, ion dose and irradiation temperature. These coated layers are useful in nuclear reactors where the environment is very corrosive and exposed to very high temperatures.

(ii) *Ion beam assisted deposition* Ion beam assisted deposition (IBAD), commonly known as double ion beam sputtering deposition (DIBS), is another surface modification technique where the physical vapor deposition (PVD) method is combined with ion implantation

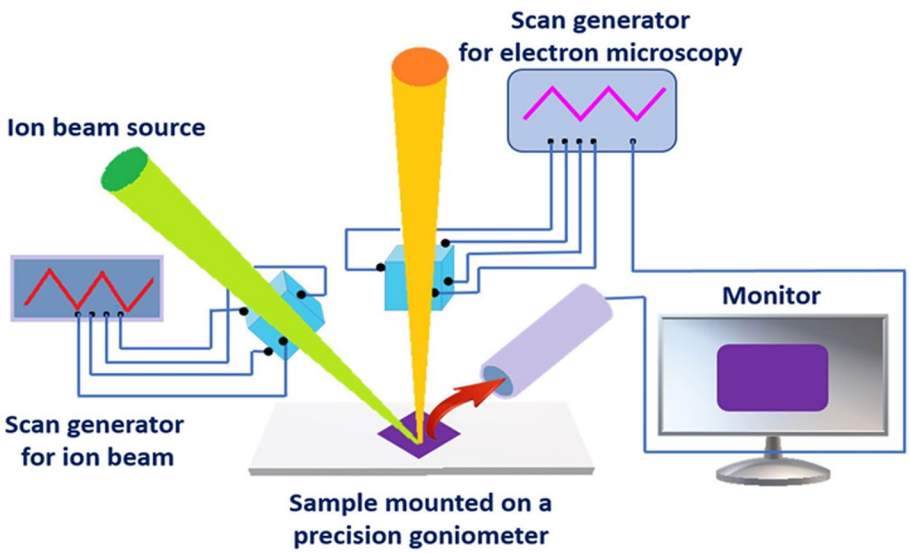


**Fig. 11** Schematic representation of the ion beam technique

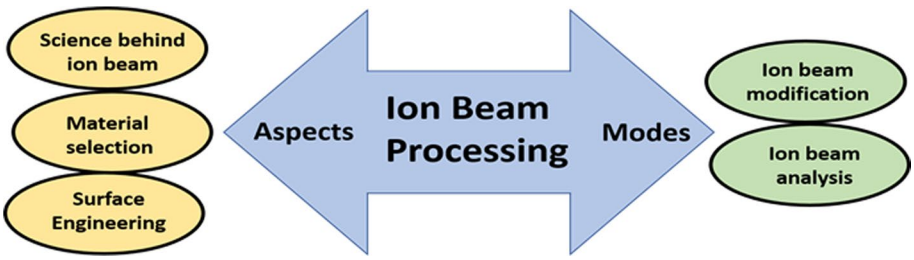


**Fig. 12** Schematic representation of ion beam processing

[123]. Here, implantation is done by inert or reactive ions. The sputtering process and ion beam bombardment are conducted simultaneously. As a result, a series of physicochemical reactions occur between the bombarded ions and deposited atoms. This dynamic mixing strengthens the properties of modified films [124]. Thus, a number of high-quality films can be made at ambient temperature using this technique [125].

(iii) *Ion beam induced crystallization and amorphization* Epitaxial crystallization of the layers may occur under specific implant conditions of ion bombardment. With high temperature and small ion fluxes, the crystal spreads into the amorphous phase and vice versa. There is a decisive balance between damage generation and its disintegration during amorphous Si formation [126]. The theoretical models provide a better realization of crystal-to-amorphous transition mechanisms [127].

(iv) *Ion implantation* Ion implantation is an ambient temperature surface treatment tool where low doses of impurities (dopants) are implanted to enhance the properties of materials such as semiconductors [128, 129]. In this process, dopant atoms are first volatilized, ionized then subsequently accelerated. They are separated by the mass-to-charge ratios and finally bombarded onto the target. Thus, dopants implant into the crystal lattice of the host atoms, and the average penetration depth is governed by the nature of the dopants, properties of target materials, and acceleration energy.

(v) *Ion beam irradiation* This is a commonly used technique for fabricating nanostructured thin films in industrial, technological, and medical applications [130]. Ion beam irradiation gives rise to new phases around the interfaces, which can improve its physicochemical properties. Irradiated ethylene tetrafluoroethylene (ETFE) films are used mainly in the technological and medical domains [131].

**3.2.1.2 Analysis of Materials by Ion Beam** The properties and performances of the surface-engineered materials are strongly governed by their structures and composition. When an energetic ion beam hits a target, numerous collisions happen. During those collisions, the incident particle loses energy. These energy loss processes capture depth information of the target from a few tens of nanometers to micrometers, which can be measured by ion beam analysis. The emission products from these ion–solid interactions play an intrinsic role in describing the surfaces and interfaces of the material composition and structure. These interparticle interactions, e.g., scattering, inner-shell ionization, and nuclear reactions, usually depend on innumerable variables, which include ion velocity and energy, size, atomic number, and mass of the solid. There are several ion beam analysis techniques available, as summarized in Fig. 13.

### 3.2.2 Advantages of Ion Beam Processing

The flexible nature of ion beams makes them suitable for quick down-selection of materials. The ion beam is generally used for etching, sputtering, irradiation, implantation, and analysis, depending upon the needs of targeted applications. As it is a low-temperature treatment process, it does not cause any thermal distortion in the material. All types of materials ranging from metals to biomaterials, can be modified or analyzed using an ion beam source. It gives outstanding uniformity, versatility, independent ion beam energy, and flexibility as achieved by precise current control, accuracy,

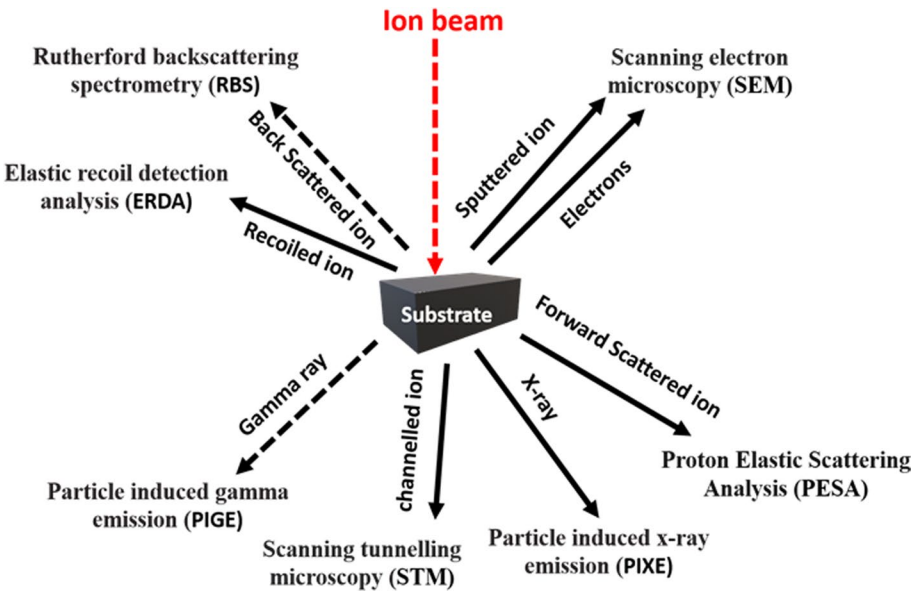


**Fig. 13** Ion beam analysis techniques

and repeatability. This provides a facile and consistent etching process. Sputtering ion beam sources are becoming more attractive in the etching process. Ion beam analysis techniques remain unparalleled in three areas: (i) light element analysis using particle-induced gamma emission (PIGE), nuclear reaction analysis (NRA), or elastic recoil detection analysis (ERDA) techniques, (ii) elemental depth profiling via Rutherford backscattering spectrometry (RBS), NRA or ERDA techniques and (iii) large-scale elemental imaging mainly based on particle-induced X-ray emission (PIXE) [132]. This flexible and highly configurable technology has numerous industrial applications [133].

#### 3.2.3 Exotic Applications of Ion Beam Technology

Innovative research for advanced surface-engineered material in exotic applications such as nuclear, offshore oil & gas and space industries is essential for smooth and safe operations. Ion beam techniques are promising and are extensively used to enhance the tribological properties of such materials. Some of the relevant research related to the applications is described in this section.

**3.2.3.1 Nuclear Industry** Nuclear energy is a promising prime source of energy as it is environmentally less damaging than fossil fuels and can supply stable baseline energy. Next-generation high-temperature gas-cooled reactor (HTGR) may be a potential candidate for hydrogen production [134] as it can withstand the high temperature (1223 K) needed in the sulfur-iodine cycle. Park et al. [135] showed the effects of ion beam mixing of a ceramic film (SiC) onto a metallic material (stainless steel and Ni-based alloys) for nuclear hydrogen production above 1173 K in a $SO_3/SO_2$ ambient. An approximately 50 nm thick SiC ceramic film was deposited by the e-beam evaporation method on 316L ASS, Inconel 800 H, 690, and Hastelloy-X substrates. After that, 100 keV (Ar and N) ion bombardment was used to mix the interfacial region. An additional 500 nm thick SiC film was deposited on the ion bombarded SiC film. A corrosion resistance evaluation was performed on samples with/without ion beam mixing by immersing in a 50% $H_2SO_4$ solution for 1 h at 573 K. It was observed that the film without mixing was completely removed, while the ion beam treated sample showed no detachment. The optical micrographs of etched SiC/Hastelloy-X surfaces revealed that non-ion beam surfaces had film flakes at the edge of the film, whereas no such observation was made in ion beam modified surfaces. This means the modified interface was protective against a corrosive environment.

The materials used in nuclear reactors are irradiated with high (fission fragments) and low (alpha particle and neutrons) energy particles. Uranium is a highly active and corrosive metal when it comes in contact with $H_2$, $O_2$, or $H_2O$. This diminishes its performance, lifetime and also its efficiency [136–138]. Cerium (Ce) can be used as an attractive reference metal for simulating uranium due to its similar electronic configuration. Liang et al. [139] investigated the improvement in corrosion resistance of Ce (simulating uranium) by deposition of TiN/CeN as well as CeN/TiN bilayer composite films using the DIBS method. The results indicated that the CeN/TiN bilayer composite film had superior resistance to corrosion. Therefore, this might be a useful shield for uranium in a corrosive environment.

Another crucial nuclear reactor material, yttria-stabilized zirconia (YSZ), is commonly used for the partitioning and transmutation of radiotoxic actinides as an inert matrix fuel [16, 17]. There is a need to understand the structural changes under the influence of radiation at an atomic level and the consequent effect on radionuclide liberation rates during corrosion. Investigation revealed that YSZ is a strongly radiation-resistant ceramic material [140]. When exposed to ion beam irradiation, it experiences atomic displacement damage and accumulates many gas atoms [129]. Zhang et al. [141] investigated the irradiation effects of ion-induced damage by Rutherford backscattering spectrometry (RBS) using a 2.022 MeV helium ion beam with 15 keV energy resolution. The results showed that displacement damage can be decreased by sequential ion beam irradiation. Additionally, a reduction of interstitial He atoms was observed, which led to a decrease in displacement damage, which is helpful for real industrial applications in nuclear reactors.

**3.2.3.2 Oil & Gas Industry** The oil & gas industry has been facing many challenges due to aggressive and extreme weather conditions. The major issues in this industry are flow-accelerated corrosion and environment-assisted cracking, as mentioned in Sect. 2. The analysis of the corrosion behavior of structural materials is necessary to avoid catastrophic failure in marine environments. Three major types of environment-assisted cracking (HE cracking, sulfide stress corrosion (SSC) and SCC) can be modified or analyzed using ion beam technology. A site-specific cracking analysis is generally done by fractography using advanced ion beam technology. This provides thorough characterization and aids in the selection of a material for such applications. The HE of steels and other metallic alloys is a major technological concern in the integrity of operating equipment (e.g., pipelines and subsea manifolds) in the oil & gas industry [142–144]. Hydrocarbon production from sour wells (i.e., $H_2S$ containing) is an ever-increasing challenge, which gives rise to the SSC of ferritic steels [145, 146]. In aqueous corrosion, hydrogen is generated during the cathodic reaction, which is diffused through the lattice and transmitted to regions of high-stress concentration, such as advancing crack tips, causing failure in the material [147]. This is further aggravated by the presence of $H_2S$. Various

mechanisms have been proposed in the past regarding the actual micromechanical pathways of failure. They can be grouped into three major mechanisms: hydrogen-enhanced localized plasticity (HELP) [148, 149], hydrogen-enhanced strain-induced vacancy (HESIV) mechanisms [150, 151] and hydrogen-enhanced de-cohesion (HEDE) [152, 153]. However, no mechanism conclusively addresses the exact science behind premature failure in the presence of $H_2$. To understand the role of hydrogen relevant to plasticity and damage, Srinivasan et al. [154] did detailed fractography of Ferritic steel using crack-tip focused ion beam transmission electron microscopy (FIB-TEM) coupled with high-resolution SEM and compared the mechanisms associated with deformation. This investigation provided possible damage evolution mechanisms in the presence of hydrogen. They proposed a unique micro mechanism method (nano-void coalescence mechanism or NVC) consisting of three stages: (i) nano-void nucleation, (ii) growth and (iii) coalescence of HE, as schematically represented in Fig. 14.

A comprehensive understanding of the proposed mechanism(s) related to HE helps to down-select a material and service condition in oil & gas industry applications [155]. DSS provides excellent resistance to intergranular degradation and excellent stress and crevice corrosion resistance along with moderate mechanical strength as compared to standard austenitic stainless steels [156]. However, it loses toughness and corrosion resistance during forging and heat treatment. Detailed failure analyses have been done by Bruch et al. [157] using a FIB device. They found that high forging ratios and strict temperature control can give excellent corrosion resistance along with high impact strength and precipitation-free microstructures in DSS.

HE can also be reduced by adding noble metals (such as copper, silver, palladium, and platinum) in $H_2S$ environments [158, 159]. Wilde et al. [160] performed palladium (Pd) ion beam mixing for surface modification and found that it significantly reduced the hydrogen absorbed fraction (HAF) as compared to non-modified surfaces. An accelerated hydrogen embrittlement test was conducted using a slow-strain rate procedure [161] to determine the HE resistance improvement in modified surfaces. Severe intergranular fracture was observed from micrographs of a non-surface treated specimen than Pd ion-beam mixed surface, which was less susceptible to HE and was fully ductile in nature. Thus, surface modification by Pd-ion beam mixing significantly reduced the hydrogen absorption and HE of steels.

**3.2.3.3 Space and Aviation Industries** Complex-shaped components in the aerospace industry are often made from materials that feature poor machinability. Surface engineering of those components demands the use of concentrated energy fluxes [162] to form a composite material with a gradient of properties. Surface coatings by ion implantation followed by ion deposition improved the quality parameters of those processes [163, 164]. Vityaz et al. [163] performed surface modification of the high-speed tool steel R6M5 using ion implantation followed by ion deposition. They observed that microhardness was increased by four times after chromium ion implantation, followed by deposition, indicating the strengthening of the material. The microstructural analysis also revealed fewer micro-cracks in the surface layers without much change in the phase distribution pattern. Hence, the surface self-organization process helps to build outer layers of required thickness over a complex-shape structure during ion beam modification.

To improve the fretting fatigue resistance of Ti–6Al–4V titanium alloy, Tang et al. [165] used ion beam enhanced magnetron sputtering deposition for preparing Ti/Mo metallic multi-layer films with different periodicities. The fretting fatigue resistance and mechanical properties (such as tribological properties, hardness, and toughness) of the optimized film were investigated. They observed that high density, small grain size, and high bonding strength films were deposited after modification. In short, the formation of Ti/Mo metallic multi-layer films using an ion beam enhanced magnetron sputtering deposition improved the toughness, hardness, adhesion, and wear resistance of titanium alloys.

Polyimides and carbon coatings commonly used in space stations require durability in space environments. They gradually erode and experience changes in their properties when exposed in LEO [33, 166, 167]. Protective coatings are required to prevent oxidation of those materials. Banks et al. [168] reported a thin film coating on polymer (Kapton®) by ion beam sputtering followed by deposition as the

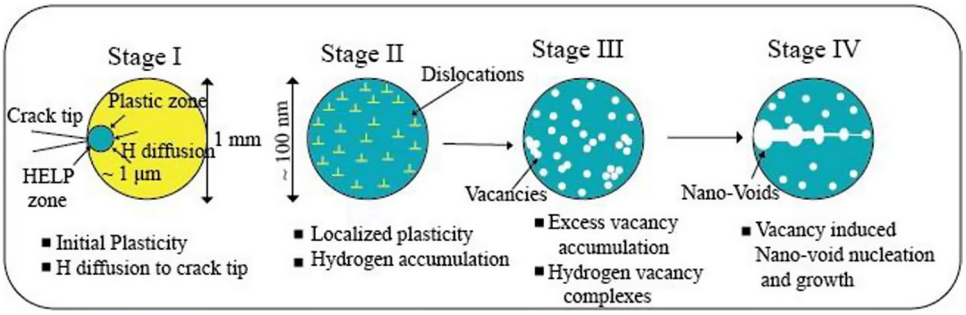


**Fig. 14** Schematic representation of stages associated with the NVC mechanism. Reproduced with permission from [154]

protection of the spacecraft in LEO. The thin films consist of $Al_2O_3$, $SiO_2$, and a mixture of co-deposited $SiO_2$ with small amounts of a fluoropolymer. The investigation of the space flight (STS-8) exposed samples revealed an effective and protective coating had been achieved using an ion beam over polyimide Kapton®.

## 3.3 Electron Beam (EB)

EB surface modification is a well-established methodology among the various surface engineering techniques due to its higher energy efficiency and precision control mechanism inside the vacuum chamber [169]. In this technique, the electrons are emitted and accelerated by electrical potentials and follow a path through the focusing lens and deflecting coils. Here, the electrons are electromagnetically deflected and further guided on the focused region of the selected material. The kinetic energy of the electrons gets transformed into heat while striking the material surface with a very high velocity, leading to the formation of thermal gradients from the surface to the bulk. The whole process is carried out in a vacuum chamber, which helps to avoid the dispersion of electron beams [170]. There are two types of EB processing techniques: continuous and pulsed. The major differences between them are the heating and cooling rates. For pulsed EBT, the cooling rate can extend up to $10^9$ K/s [171], while in the continuous mode, it is about $10^5$ K/s [142], leading to various properties of materials.

### 3.3.1 Advantages of EB Surface Treatment

Electron beams (EBs) have been extensively studied as surface engineering tools in various industries, especially exotic applications, where improved surface properties are desirable. Some of the most convenient aspects of this technology are mentioned below [170–173]:

(I) EB produces very high surface temperature without consuming much energy compared to conventional methods. The process is very effective for large-scale processing and may save up to 40% of the total energy consumption.
(II) EB processing takes a comparatively shorter processing time than the other surface engineering techniques.
(III) Better surface finish, higher-order dimensional accuracy, and contamination-free surfaces are the most advantageous features of EB surface engineering.
(IV) This technology can be used for highly reactive materials, as the entire process is executed inside a vacuum chamber.
(V) EB has high precision and uniform distribution of energy throughout the surface of the material.

### 3.3.2 EB Techniques

EB surface engineering techniques include EB-induced surface hardening, alloying, melting, and cladding. Some structural changes and phase transformation might occur if the workpiece surface temperature reaches its melting point. The EB processing technique is schematically represented in Fig. 15. Among the numerous EB processing/surface engineering techniques, some essential procedures are discussed below.

**3.3.2.1 EB Surface Hardening** EB surface hardening is used to improve the surface properties of the materials, primarily the surface hardness. Here, the specimen is heated above the plasticization temperature (lower than the melting point), followed by rapid cooling resulting in a fine crystalline microstructure related to the higher surface hardness. This method is widely used in industries where hardened materials are required [173].

**3.3.2.2 EB Alloying** This method can be exploited to form a distinct surface alloy when compared to the base material, leading to superior functional properties. Due to the high energy of electrons, the EB exposed area quickly reaches the material's melting point, causing localized melting in a contaminant-free environment. This ensures a proper distribution of alloying elements in the melt pool, which forms the surface alloy upon solidification. The EB alloying technique

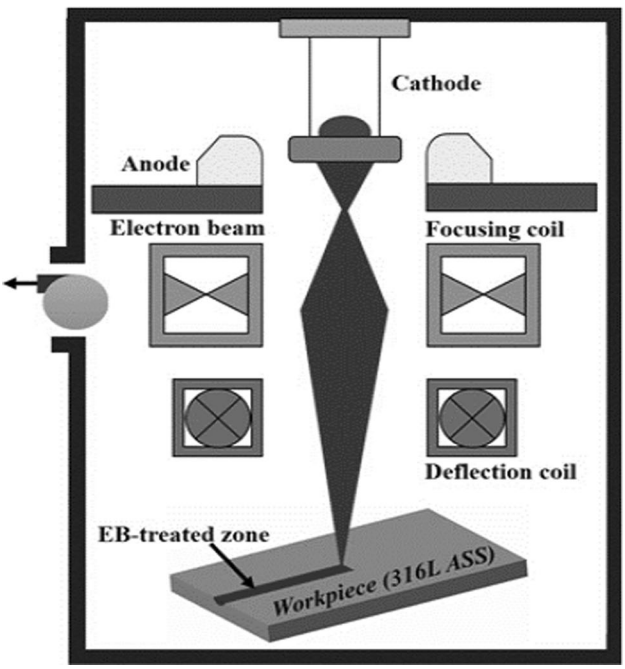


**Fig. 15** Schematic representation of EB processing on the structural material

is a rapid surface engineering tool that could be used in many exotic applications. Still, this method is significantly more appropriate for improving surface properties of lighter metals and alloys like Ti and Al [174].

**3.3.2.3 EB Melting** In this process, high velocity electrons are generated by applying high electrical potential. These electrons are tightly focused using magnetic fields. When the electrons strike the sample material during EBM, the kinetic energy is converted into heat or thermal energy. Thus, this procedure occurs above the melting temperature and melts the surface layer [174].

**3.3.2.4 EB cladding** EB cladding is essentially powder freezing in the liquid metal pool induced by EB. In this process, a feeder is used for feeding the cladding powder inside the molten pool of the substrate materials. Under the influence of EB, the cladding powder is melted and solidified, forming a good metallurgical bond. During this process, EB parameters and other conditions must be precisely optimized. Some of the industrial applications of the EB cladding procedure are surface hardening, crack/porosity filling and tool repair [175].

### 3.3.3 EB in Exotic Applications

Surface engineering technologies related to EB are used in exotic applications to enhance the mechanical and surface-mechanical properties of the desired materials. Different EB treatment procedures, such as EB surface hardening and EB alloying, are used to address surface-related challenges in harsh environments. This section primarily focuses on some of the recent developments in EB surface treatment techniques for aerospace and nuclear applications.

**3.3.3.1 Aviation Industry** Ti, Al–Si, and Mg alloys are materials widely used in aviation industries to manufacture various components such as airframes, landing gears, blades, tubes of fuel tanks, and engine parts. However, these materials have some drawbacks, like low hardness and poor corrosion/wear resistance. These could be effectively addressed through advanced surface modification techniques such as EB treatment technologies. Recent works related to EB surface treatment for Ti, Al–Si, and Mg alloys are discussed below.

Hao et al. [176] performed a high-current pulsed electron beam (HCPEB) technique on Mg alloy (AZ91) to examine the improvement in microhardness and corrosion resistance as a function of electron pulses. They reported that after three pulses of HCPEB, the β-$Mg_{17}Al_{12}$ phase melted and dissolved into the surrounding matrix. After fifteen pulses of HCPEB, a very flat surface (depth ~ 8 µm) was obtained with the complete disappearance of the β-$Mg_{17}Al_{12}$ phase. They concluded that rapid solidification inside the melt pool was the primary reason for the changes in microstructures, which resulted in improved strength and surface hardness after 30 pulses of HCPEB. Furthermore, they found that the mechanical properties of the treated alloy increased proportionally with the number of pulses. Still, the corrosion resistance was maximum only after 15 pulses of HCPEB treatment.

Walker et al. [177] studied large-area pulsed electron beam melting (LAEBM) on the surface morphology and electrochemical behavior of Ti–6Al–4V alloy. The alpha prime martensitic phase appeared after rapid cooling induced by this treatment. The corrosion rates of LAEBM treated samples are significantly lower (by order of approximately 150 times during a 15 pulse treatment) than the untreated samples. Such considerable improvement in corrosion behavior can be attributed to a homogeneous martensitic layer that facilitates a dense passive oxide layer during electrochemical testing.

Gao et al. [178] examined the impact of the pulsed EB-technique on the titanium (TA15) alloy surface and investigated the hardness distribution on the treated surface. The authors reported that the hardness on the surface melt layer (~ 25 µm) was significantly higher due to the fine grain microstructure and lower heat effect. Zagulyaev et al. [179] examined the EB-pulsed technique on the microhardness and the tribological behavior of a Si-rich Al alloy (silumin). The maximum drop in wear properties and maximum increase in microhardness were found at energy densities of 35 J/$cm^2$ and 30 J/$cm^2$, respectively. Post-treatment SEM studies revealed that the silumin surface layer was homogeneous. The surface layer thickness varied from 35 to 80 µm depending on the input energy densities, and inclusions of dimensions between 150 and 175 nm were homogeneously dispersed throughout the surface layer. Guo et al. [180] examined the wear and corrosion resistance of Ti–6Al–4V alloy irradiated by HCPEB. The surface roughness of the irradiated samples decreased as the number of pulses increased due to the disappearance of crater-like morphologies. However, the surface roughness was still approximately ten times higher compared with the untreated samples. The corrosion potential ($E_{corr}$) of treated samples increased from – 709 mV (N = 0) to − 202 mV (N = 5), demonstrating an increase in corrosion resistance.

**3.3.3.2 Nuclear Industry** Inconel 617 and 316L ASS are extensively used materials in nuclear applications due to their high-temperature mechanical and tribological properties, including wear and corrosion resistance. These materials are candidate structural materials for fuel-cladding tubes, steam-generator tubes, and various nuclear reactors like pressurized water reactors (PWR) and very high-temperature reactors (VHTR) in nuclear energy applications [181]. Irrespective of their performance, high stress (residual, ten-

sile, or both), temperature, pressure, and very aggressive (toxic) environments for nuclear power generation demand compulsory enhancement of the surface properties of these service materials.

In pursuit of nuclear energy applications, Basak et al. [182, 183] conducted EB melting/surface treatments on Inconel 617 superalloys and 316L ASS. In the case of Inconel 617, they reported that the processed region was separated from the substrate with a solid–liquid interface boundary. The columnar dendritic microstructure revealed inside the melt pool resulted in higher surface hardness than the base material condition. Post EB-treated material showed higher corrosion resistance than the base material. The development of the properties was mainly due to homogenized microstructures, grain size reduction and purification of the surface layer by EB irradiation [183].

For the 316L ASS substrate, the same research team clarified some specific reasons for the improved tribological properties observed in the EB-treated sample. The higher amounts of thermal stress and the formation of fine dendrites inside the EB-treated region enhanced dislocation density and hindered its movements. The fretting wear rate was also observed to be very low in EB-treated samples due to the development of fine microstructural properties and increased microhardness. The dendritic microstructures with significant grain refinement showed improved corrosion resistance in passive electrolytic solution compared to the unprocessed region coarse-grained microstructures [182].

## 3.4 Plasma Immersion Ion Implantation (PIII)

PIII is another promising and versatile surface engineering method for various substances, including semiconductors, metals, insulating materials (polymers, ceramics, and rubber) and dielectric materials [184]. In the mid-1980s, PIII was first demonstrated by Conrad et al. [185] and Tendys et al. [186], who enhanced the capabilities of the conventional ion implantation (CII) technique by addressing technical complexities, non-uniform implantation on complex-shaped three-dimensional (3D) targets (tools, dies, and mechanical parts), and higher cost. The technical advancement of the PIII technique compared to the CII method is discussed below.

### 3.4.1 Working Principle of Conventional ion Implantation (CII)

The CII technique used to be a preferred choice for enhancing surface properties like wear, corrosion, fatigue performance of materials, and selective doping of silicon wafers for semiconductor applications [187]. As shown in Fig. 16a, ions of desired materials are extracted effectively from the plasma of ions source in CII and are focused to form a collimated beam using a set of extraction grids. The ions in the collimated beam are accelerated to achieve the desired energy after passing through the beam rastering system. They are then scanned across the target surface for uniform implantation. As CII is a line-of-sight technique, a manipulator stage with a sophisticated computer-controlled system is also required for a non-planar target to rotate, which uniformly implants all sides of the target in the presence of an adequate heat sink.

Target manipulation is an additional complex and costly aspect that also imposes target size constraints making it more difficult to achieve uniform implantation. In addition, target masking (Fig. 16c) in CII is required to maximize the retained dose by minimizing the ion beam incidence angle (Fig. 16b) to less than 20°–30°, which otherwise causes undesired excessive sputtering that further aggravates the design complexity and increases the cost of the system. Additionally, sputtering of the mask might lead to contamination of the target [185, 188, 189]. An advanced PIII technique can address those issues and, therefore, can complement the CII for the surface treatment of large, complex 3D parts or samples.

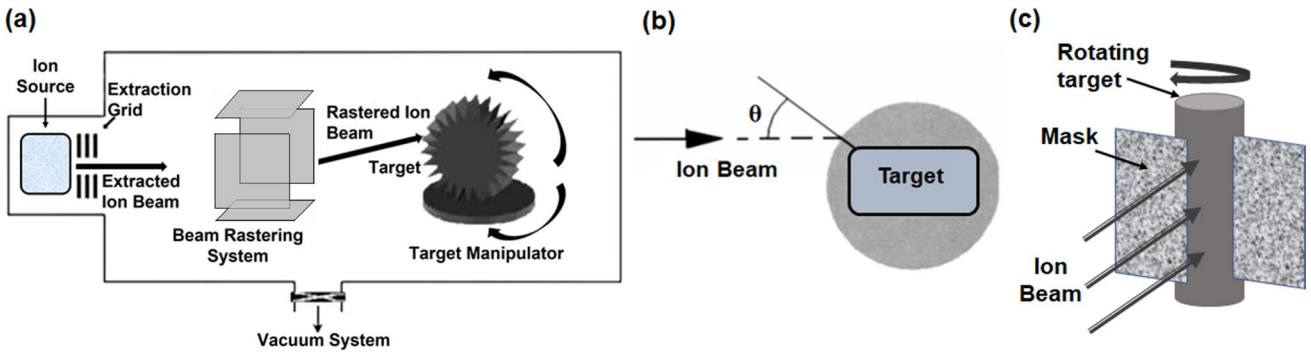


**Fig. 16** Schematic presentation showing **a** the principle of the CII technique, **b** retained dose issues due to the incidence angle of the beam. **c** Masking of convex targets in CII to minimize the sputtering of ions and to maximize the retained dose. Adapted from [187]

#### 3.4.2 Working Principle of Plasma Immersion Ion Implantation (PIII)

In the PIII technique [185, 188, 189], target materials/components are placed directly inside a vacuum chamber where the targets are subjected to plasma ions to be implanted (Fig. 17). The targets are then negatively pulse biased (~ KV) while the chamber wall is grounded. As a result, the enforced negative potential repels the electrons further from the target towards the chamber walls, forming a positive ion plasma sheath surrounding the target. Therefore, ions are accelerated in all directions normal to the target surface due to the potential difference across the plasma sheath. This leads to uniform implantation from all sides (Fig. 17b). Thus, PIII addresses the line-of-sight and "retained dose" requirement of CII. Additionally, PIII achieves the same goals without using complicated and sophisticated mechanisms, i.e., the ion accelerator stage, raster-scan apparatus and target-manipulator hardware, leading to a simpler, smaller, and less expensive "in-house" operation technology. Some of the advantages of PIII are:

(i) A large number of parts, irrespective of shape, size and weight, can be processed effectively at the same time and at significantly lower processing temperatures than other techniques. This makes PIII a batch-processable technique that is also beneficial for parts where an increase in temperature causes distortion of parts or degradation of microstructure and properties. The dose uniformity is also sufficiently good in batch processing or in implanting non-planar targets [190].
(ii) Surface properties (like microhardness and wear) are improved by efficiently inserting ions to the desired concentrations and depths for modifying the surface without affecting the microstructure, elemental composition and mechanical properties of the substrate materials [188].
(iii) By altering the implantation energy and the time of implantation, the concentration of the implanted ions on the target material can be changed very easily. This process generates intermetallic compounds and high concentration solid solutions, which substantially enhance the strength of the material by solid solution strengthening mechanisms [191].
(iv) Use of metal mesh-assisted PIII in insulating materials boosts the energy and the dosage of implantation by accelerating ions from the plasma, and it also eliminates the surface deformation in insulating materials [192].

PIII is also used as a hybrid technology that offers the combined benefit of PIII with deposition (PIII&D) for various coating-related applications like massive diamond-like carbon (DLC) film coatings inside cavities or holes, the inner surface of metallic pipes and tubes used in oil & gas industries, in rocket engines to be used in space exploration, in the aerospace industry as fuel feeding and refrigeration tubes, and in the nuclear industry as liquid transporting pipes in fission and fusion devices [193, 194]. The PIII process is also used in an ion beam enhanced deposition (IBED) mode to develop metal alloys or various coatings such as metal nitride coatings [190]. PIII with a metal plasma and cathodic arc deposition represents another method for ion implantation with film deposition protocol, referred to as metal plasma immersion ion implantation and deposition (MePIID). Metal plasma also includes plasmas of semi-metallic and semiconductor materials (C, Si and Ge), which can be used in the deposition of non-crystalline carbon in magnetic recording heads [195, 196].

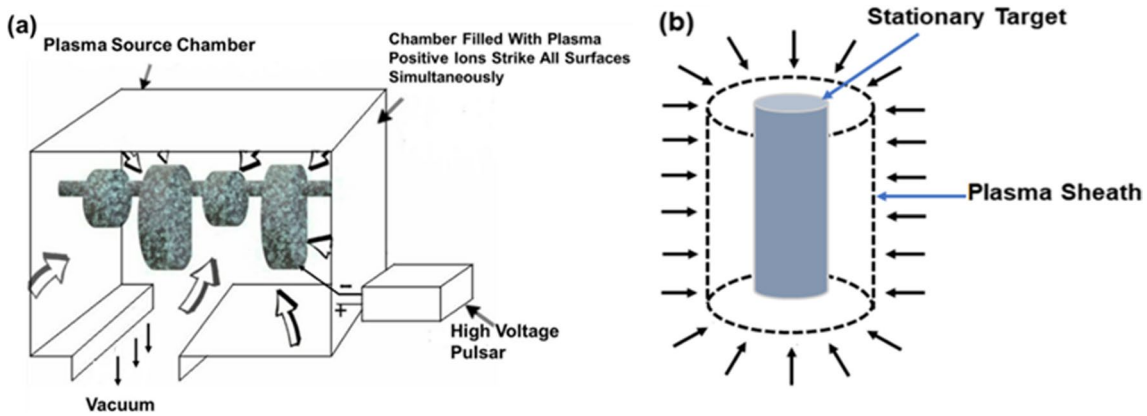


**Fig. 17** Schematic diagram depicting **a** PIII technique, showing plasma sheath surrounding the target followed by the plasma ion bombardment. This eliminates the requirements of rastering of the beam or specific target adaptations. Reproduced with permission from [189]. **b** Normal incidence of plasma ions over the target surfaces in PIII eliminates the need for masking. Adapted from [187]

Despite having few drawbacks (like no mass separation, which causes implantation of contaminants present in the plasma, the secondary electron problem, generation of X-rays, inaccurate monitoring of in situ dose, inhomogeneous distribution of implantation energy) [193, 194], PIII has attracted greater attention as a promising technique for surface engineering from both researchers and industries.

#### 3.4.3 Application of PIII in Exotic Applications

There is always demand for advanced surface modification techniques with higher performance in many exotic applications like nuclear, space, aviation, oil, and gas industries. Various requirements like less capital investment, easy operation and maintenance of the system, high throughput, and longer lifetimes of manufacturing tools push adoption of the PIII technique for exotic applications.

**3.4.3.1 Nuclear Industry** Advanced applications in the nuclear industry demand new materials/alloys or surface modification of existing materials/alloys to improve their performances to (i) protect products against HE in water-cooled nuclear reactors, (ii) provide more complete fuel burn up and (iii) improve the safety of nuclear reactors.

Long et al. [197] reported that the nitrogen implantation of uranium metal by the PIII process increases the lifespan of uranium as it can significantly improve corrosion resistance and can effectively prevent surface oxidation for longer durations, even in adverse environments. Severe corrosion on the untreated sample after 3 months of exposure to challenging environments was reported, whereas the implantation sample revealed only the emergence of micro-pits on the surface and occurrence of dot-corrosion around the edge of these pits. The depth profile analysis of the sample kept in a hot and humid atmosphere using auger electron spectroscopy (AES) showed that the untreated uranium undergoes acute corrosion only after one month due to continuous diffusion of oxygen to the uranium substrate. However, the implantation sample indicated a very weak oxygen and nitrogen diffusion in the modified layer even after three months in an adverse environment. A nitride layer formed on the surface, preventing oxygen diffusion. Thus, the original morphology of the modified layer remained unchanged.

Kashkarov et al. [191, 198–200] conducted a few studies regarding the protection of Zr-alloys (Zr-1Nb, Zr-2.5Nb) using cladding (as mentioned in Sect. 2.1) against HE by Ti-implantation using the PIII process. After hydrogenation of the treated Zr-alloys for 60 min under a hydrogen atmosphere at 673 K and 2 atm hydrogen pressure, they observed a decrease in hydrogen sorption rate and improved mechanical properties of the Ti-implanted Zr layer at higher bias voltage (1000 and 1500 V) because the Ti had a minimal neutron capture cross-section, increased melting point and substantially higher resistance to corrosion [191, 199]. The structural analysis of the samples after hydrogenation revealed only the presence of hexagonal α-Zr phase without any Zr hydride phase in the Ti-modified samples treated at 1000 V and 1500 V. This was in contrast to the unmodified sample and sample modified at 500 V, which showed the existence of a minimum amount of titanium hydride ($TiH_2$) and δ-zirconium hydride ($ZrH_{1.66}$) phases. The glow-discharge optical emission spectroscopy depth distribution study of elements after hydrogenation also indicated less penetration of hydrogen into the Ti-implanted sample at higher bias voltages than the initial and 500 V bias Ti-implanted sample. The modified surface layer at higher bias voltage trapped the hydrogen due to interactions between vacancy-type defects, which were created by the bombardment of the initial surface with accelerated ionized clusters. The Ti-implantation formed a barrier layer against the penetration of hydrogen into Zr-1Nb alloy. This significantly enhanced the corrosion-resistance and mechanical and tribological properties of the treated alloy, which prevented embrittlement of Zr-alloys cladding in nuclear reactors to a greater extent. Kashkarov et al. [198] also reported improved mechanical properties of Zr-2.5Nb alloy by Ti ion implantation using PIII.

**3.4.3.2 Offshore Oil & Gas Industry** A few studies about surface modification of large complex-shaped industrial components (e.g., pistons, rings, and pipes) using PIII were reported that illustrate the long-term application of the components in the hostile environment (discussed in Sect. 2.2) relevant to the oil & gas industries.

Wang et al. [201] investigated the surface modification of a steel piston column of irregular shape and large dimensions typically utilized in oil pumps to extract crude oil. The lifetime of the oil column was increased by radio frequency (RF) plasma nitriding treatment using a RF plasma source in combination with IBED, followed by nitrogen immersion ion implantation. The RF plasma source diffused the implanted nitrogen ions deeper into the substrate to form a thicker modified layer. The subsequent sputter deposition of Ti and nitrogen PIII formed a passivation layer on the treated sample that tremendously increased the microhardness of the treated sample. Along with microhardness, the mass loss due to wear and the coefficient of friction of the treated sample decreased drastically compared to the untreated sample. The untreated sample indicates severe rusting after only 30 min of the salt fog test, while the treated sample shows only 4% rust after 8 h of the test (Fig. 18).

Austenitic UNS S31254 and Duplex UNS S32205 SS are extensively used in components exposed to seawater as the presence of nitrogen and high contents of Cr, Mo, and Ni increase their resistance to pitting corrosion. Martensitic UNS S41426 SS is highly recommended in 'oil country

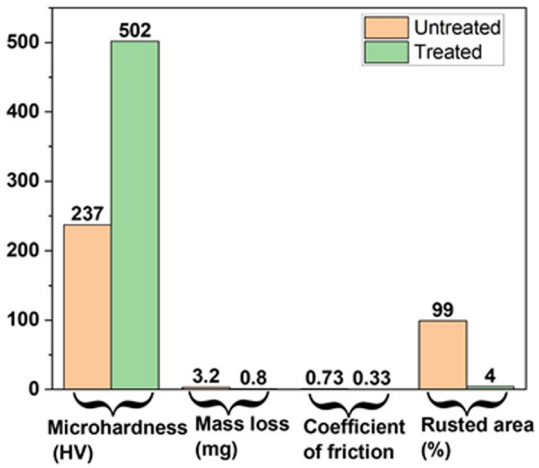


**Fig. 18** Comparison of microhardness, mass loss due to wear, coefficient of friction and salt fog test results of untreated and treated samples [201]

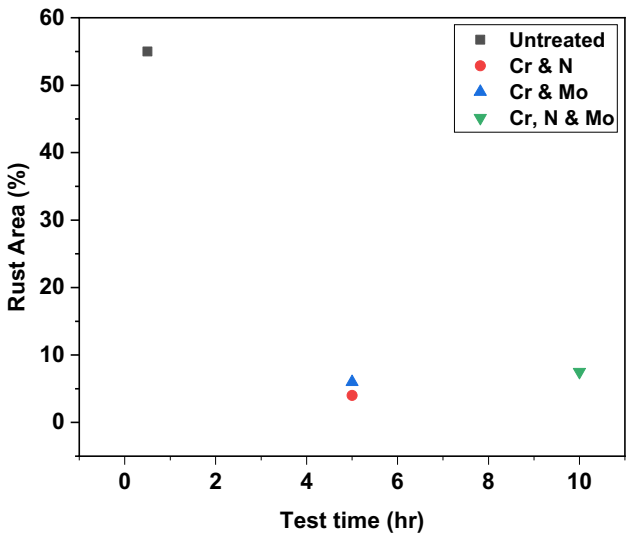


**Fig. 19** Salt fog test results of untreated and treated $Cr_4Mo_4V$ samples in 0.1 M NaCl solution [27]

tubular goods,' i.e., drill pipes (used in drilling), casing (stabilizes the wellbore) and tubing (production and delivery tubes used for the transportation of the oil/gas to the surface) utilized in oil/gas production. Ferritic UNS S44400 SS is primarily used in heat exchangers, valves, and piping systems. Luiz et al. [20] performed nitrogen implantation using PIII to improve the corrosion and wear resistance of these four types of structural materials. After nitriding, all the SS samples exhibited enhanced properties such as high hardness (> 1000 $HV_{0.01}$) and excellent corrosion resistance during 30 days of immersion in 3.5% NaCl. The passive film polarization resistance ($R_{P30}$) and trans-passive potential ($E_{tr}$) also increased by 770% and 200%, respectively. It was observed that nitrogen implantation did not change the inherent corrosion resistance of these materials. Instead, it enhanced the protection mechanism of the already present passive film by improving the diffusion and charge transfer process. Mariano et al. [194] demonstrated the effective deposition of DLC films (remarkable corrosion and wear resistance, high hardness, very low friction coefficient and roughness) inside hollow AISI SS304 cylindrical tubes used for the transportation of fluids. This was achieved in the presence of a magnetic field that enhanced the confinement of plasma within the metallic tube in a PIII&D system. The inner surface needed modification against corrosive wear caused by the deposition of salt scales, and the coating of a DLC film boosted the tribological properties of the sample. Ueda et al. [193] and Kurelo et al. [202] modified the internal surfaces of metallic tubes of SS304 and super martensitic stainless steel by forming a nitride coating using PIII. These components have applications in the extraction of subsea oil. The nitride-rich coating obtained by a nitrogen solid solution improved the mechanical, tribological properties and surface resistance against abrasion.

**3.4.3.3 Space and Aviation Industries** The space and aviation industries benefit from cost-effective, rapidly advancing surface modification treatment using the PIII technique, which can increase the operating life of components without compromising safety.

Wang et al. [27] observed improved corrosion properties of $Cr_4Mo_4V$ bearing steel used as engine bearings in the space and aviation industries by introducing Cr, Mo, and/or N using the PIII technique. Figure 19 indicates that the untreated sample undergoes severe rusting after only 30 min in 0.1 M NaCl solution, whereas the rust (corrosion) resistant properties in treated samples were significantly better even after 10 h. Nitrogen implantation improved the material wear and corrosion resistance by enhancing the formation of a super hard phase in the near-surface region, Cr implantation forms $Cr_2O_3$ and $Cr(OH)_3$ phases to protect the materials, and Mo forms molybdic acid radicals and molybdenites to stop the penetration of Cl by tying up the free chlorine atoms. Also, the coefficient of friction of the treated sample decreased from ~ 0.7 to ~ 0.2.

Uda et al. [29, 30] and Tan et al. [32] investigated the treatment of polymeric materials, i.e., Kapton® (polyimide), Mylar (polyethylene terephthalate), propylene, polyethylene and silicon, used as spacecraft components in satellites/space stations orbiting in LEO. A protective coating of a fine metal oxide layer was applied over the polymers surfaces by implanting aluminum using the PIII technique for enhanced protection of the polymer samples from highly reactive atomic oxygen and vacuum ultraviolet radiation from the sun. This was achieved with a straight magnetic filter without altering the morphology

and without any contamination. The surface modification resulted in negligible mass loss during the exposure of the surface modified polymers to RF oxygen plasmas.

## 3.5 Friction Stir Processing (FSP)

### 3.5.1 Overview of FSP

FSP is an emerging solid-state surface modification technique adapted from friction-stir welding, where the revolving tool plunges and travels inside the material to achieve local microstructural changes to improve material properties, including strength, ductility, and toughness [203–206]. Shortly after its invention, FSP emerged as a preferred facile surface engineering method for lightweight structural alloys, where heating to an elevated temperature is a significant concern. FSP is used for various purposes, such as achieving microstructural homogeneity, modifying surface hardness, fabricating hybrid and in-situ surfaces and bulk metal matrix composites of Al, Mg, Cu, and other materials like high entropy alloys. In many cases, it has been used as a surface repairing technology for defective fusion weld joints. The occurrence of fusion defects could easily be avoided/filled due to the apparent flow of the materials during FSP [204, 207].

### 3.5.2 Working Principle of FSP

The tool used in FSP has two significant parts: (i) a tool pin and (ii) a tool shoulder. During the process, the tool pin plunges inside the material until the tool shoulder touches the desired facial plane of the working material and then it traverses farther to the desired path. Frictional heat is generated between the workpiece and the tool, which causes plasticization of the target material around the pin without reaching its melting point [208–210]. The rotational and translational motions of the tool control materials flow from the front of the pin to its back. The materials undergo significant plastic deformation at elevated temperatures, leading to dynamically recrystallized (DRx) refined grain structures [211–213]. The details of this solid-state surface engineering/processing technique are schematically represented in Fig. 20. After performing FSP, three different regions have formed, which are distinctly identified as a base metal (BM), thermo-mechanically affected zone (TMAZ) and stir zone (SZ).

### 3.5.3 Factors Affecting FSP and its Advantages

A few factors that affect FSP results are mentioned in the flow chart in Fig. 21. Tool geometries, particularly those of the shoulder and pin, influence process development by controlling the localized heating and material flow.

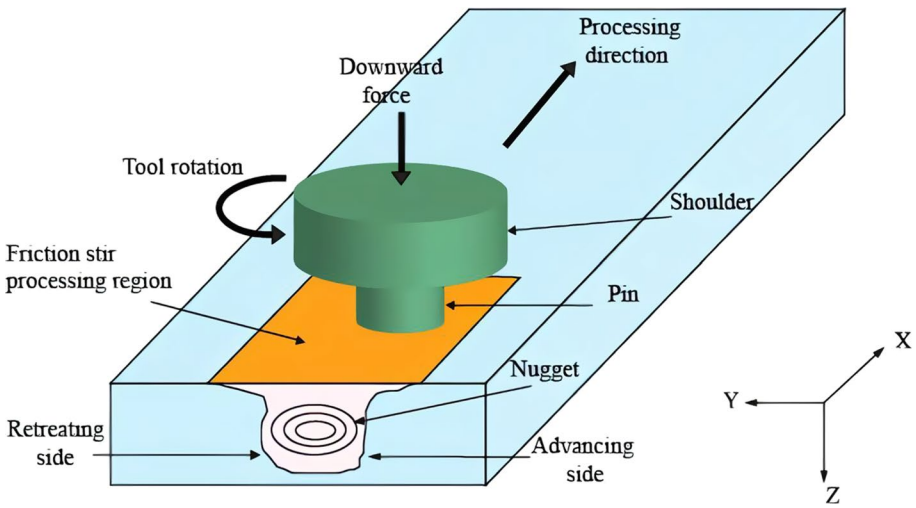


**Fig. 20** Schematic representation of FSP technology. Reproduced with permission from [213]

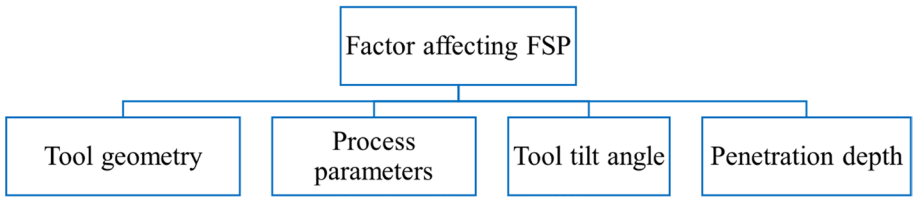


**Fig. 21** Flow chart of the factors affecting FSP

Processing parameters (such as tool-rotational speed and tool-traverse speed along the pre-specified line) also produce sound surface modifications. The amount of frictional heating increases with increasing tool-rotational speed, which results in severe stirring and a significant amount of material mixing inside the material. However, the frictional coefficient at the interface varies with tool rotational speed and its linear velocity [214]. In FSP, higher tool rotational speed caused more frictional heating than lower tool rotation while keeping the travel speed constant. Similarly, a higher tool traveling speed causes less heating than a lower travel speed in a fixed tool rotation. Selecting suitable processing parameters is crucial for determining the changes in the as-received material. Factors like the tool tilt angle and depth of penetration of the pin into the workpiece are also crucial for excellent processing outcomes. If the tool penetration is low, the tool shoulder will not meet with the exposed facial plane of the workpiece, and if it is too large, the shoulder plunges into the workpiece, resulting in a high degree of material removal [215].

Some general advantages of FSPs are [203, 207, 216]:

(I) FSP is easily performed in the case of structural materials with lower melting points.
(II) Processing temperatures near the plasticization temperature of the materials require less energy consumption during processing.
(III) Grain refinement is significant through dynamic recrystallization.
(IV) FSPs result in fewer chances of finding macroscopic defects and the porosities are almost nil.
(V) FSP provides excellent control of the system while plunging inside the material surface. Slow and fast processing could be possible based on the desired properties requirements.
(VI) Multiple types of reinforcements can be mixed with ease to produce hybrid composites.

#### 3.5.4 Applications of FSP in Exotic Applications

In space and aviation industries, aluminum alloys are promising candidate materials because of their desirable and superior properties like low density, recyclability, ductility, formability, and corrosion resistance [216–219]. However, their relatively low strength restricts the use of aluminum alloys in various fields. Also, defects like porosity inside cast aluminum alloys restrict their direct use in industries. FSP is preferred for low-melting alloy applications in aviation and space industries because it is a well-controlled surface engineering technique [213].

Wang et al. [220] reported the microstructural evolution of as-cast 2A14AA by applying multi-pass friction stir processing (MP-FSP) with 100% overlap with each other. Due to severe heat and strain generation in the MP-FSP, the microstructure of the substrate material was modified with profound plastic deformation. This process effectively produced dynamically recrystallized fine equiaxed grain structures in the SZ. As shown in Fig. 22, the average grain sizes after one-pass and two-pass remained similar while slightly increasing after the third-pass. Although the amount of dynamic recrystallization varied with the number of passes, it was mainly related to the heat generated during the processing. Additionally, they observed that the two-pass FSP processed surface achieved better strength, hardness, and ductility than the base material and other processing conditions because the combination of grain refinements and a significant amount of dynamic recrystallization effectively worked together.

Karthikeyan et al. [221] performed FSP on cast 2285AA with varying tool rotation and travel speeds. Their efforts resulted in minimizing common types of casting defects (like porosity, cavity, and small holes) due to continuous interactions between the rotational tool and the material surface through FSP, as shown in Fig. 23. They reported that the average grain size of 350 nm was changed to 400 nm as the tool rotation was reduced from 1800 to 1400 rpm with a constant tool traveling speed of 15 mm/min. However, they found better mechanical and surface properties over the parent material when processing with a lower tool travel speed (12 mm/min) at 1800 rpm. It was revealed that higher tool rotational speed ensured profound material deformation, inducing recrystallized grains inside the SZ during FSP. The temperature increase also played a vital role in material mixing and homogenization of the grain structure. The significant grain refinement of the processed materials finally improved mechanical properties over the parent material.

Sutton et al. [222] used FSP differently for nuclear-fuel storage systems. The ASS (304 or 316) made DCSS was identified with chloride stress corrosion cracking (CSCC) in-service conditions. They explained that the massive amount of residual stress present inside the fusion-welded joints of DCSS during its fabrication was primarily responsible for this cracking when it was installed near a salt-bearing environment. Chromium-carbide precipitation within the HAZ of the ASS was another reason for the observed cracking. Here, FSP was employed after the fusion weld joints of ASSs to remove the effect of sensitization at HAZ along with mitigation of DCSS surface cracking. Temperature-controlled

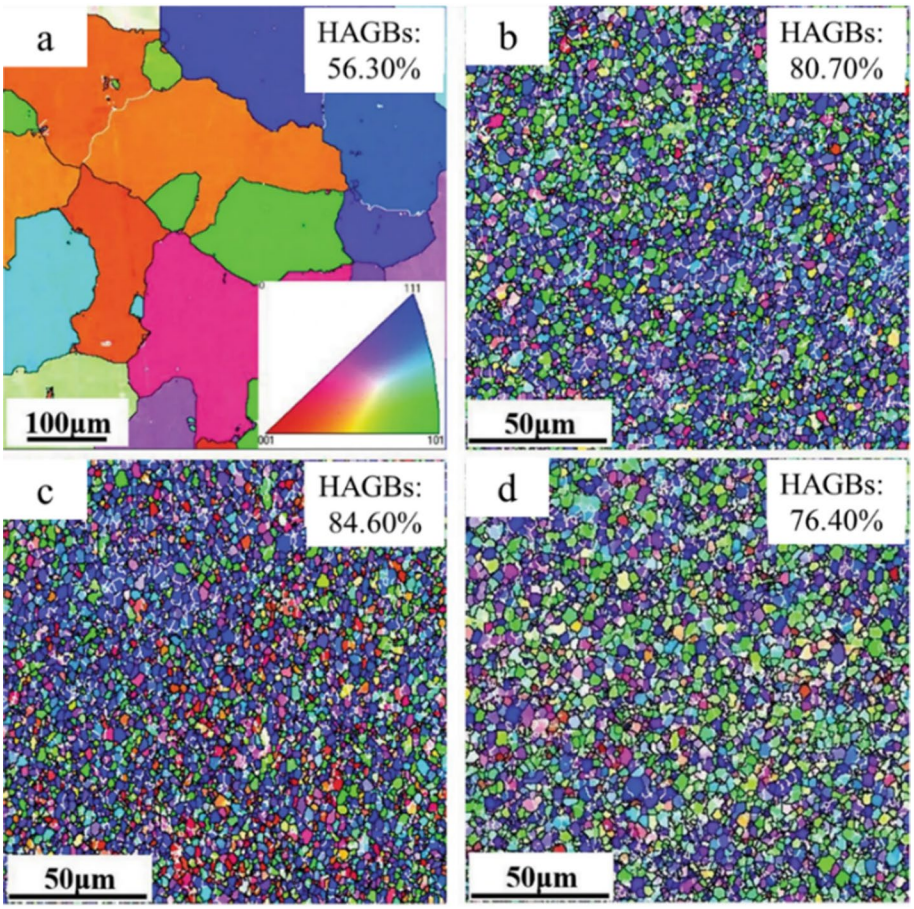


**Fig. 22** EBSD generated inverse pole figure maps representing grain sizes of 2A14AA for cases of **a** BM, **b** 1 pass FSP, **c** 2 pass FSP, and **d** 3 pass FSP. Reproduced with permission from [220]

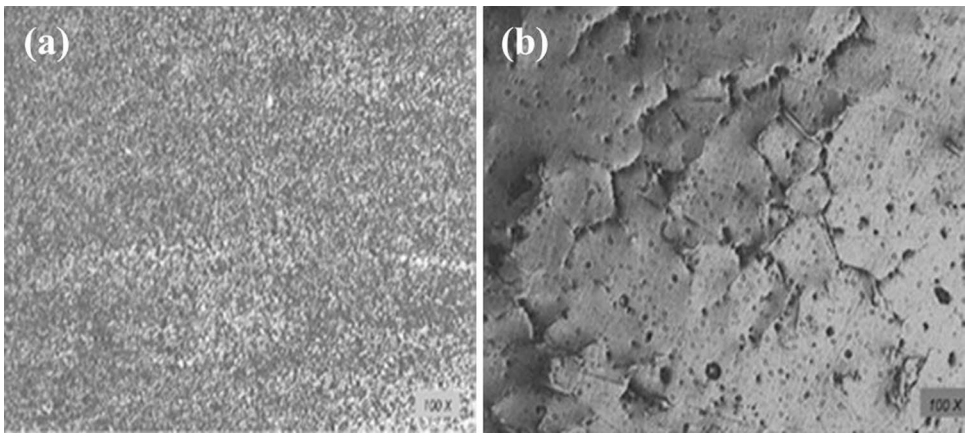


**Fig. 23** Optical microscopic images of 2285AA: **a** after FSP with refined, **b** apparent defects in as-cast condition. Reproduced with permission from [221]

FSP was applied to furnace sensitized and laboratory-generated CSCC containing 304 ASS, which was inspected after processing. This study recommended FSP as an option for repairing SCC cracking and further sensitization remediation for ASS, as the crack was fully consumed in (Fig. 24) after a single pass of FSP on the cracked materials (304 ASS).

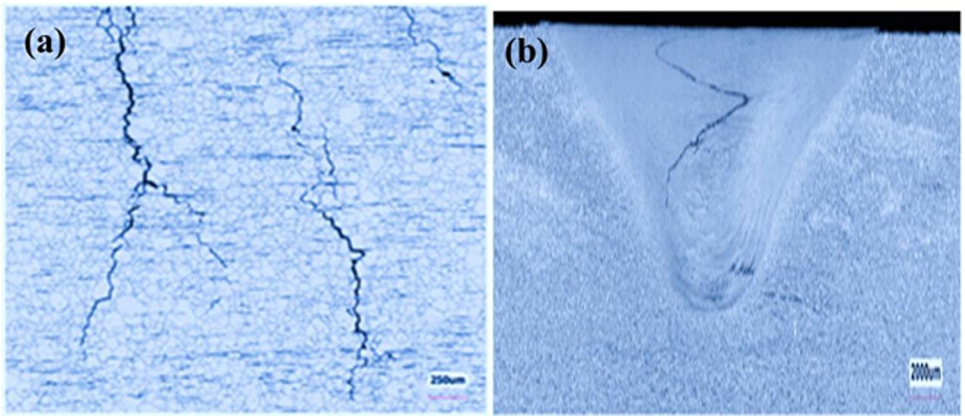


**Fig. 24** **a** Microstructure of laboratory-generated CSCC cracking inside 304 ASS, **b** macrograph of entirely consumed CSCC cracking after 1 pass FSP. Reproduced with permission from [222]

**Table 1** Summary in brief of the discussed surface treatment techniques

| Surface treatment techniques | Promising characteristics |
|---|---|
| Laser processing | A very economical precision technique, altering surface phenomena without changing the bulk properties of materials |
| Ion beam processing | A high-speed, non-destructive low-temperature surface engineering technique helps down-select materials for industrial equipment |
| Electron beam processing | An efficient surface engineering technique helps to process all kinds of materials inside a vacuum chamber |
| Plasma immersion ion implantation | A cost-effective technique can evenly implant ions on a complex 3D target for required changes in material characteristics |
| Friction stir processing | A solid-state surface processing technology helps to get microstructural homogenization (DRx) associated with mechanical properties developments |

## 4 Conclusions

This paper provides an overview of some of the most advanced surface engineering techniques that deal with exotic applications (e.g., nuclear, oil and gas, aviation, and space industries). The following conclusion can be drawn based on the comprehensive review of the technologies discussed in this article. Along with that, for ease of understanding of the technologies discussed in this article, Table 1 lists the most promising factors regarding these surface treatment technologies briefly.

(1) Laser is an economical process to alter the tribological properties of the materials without affecting their bulk. It decreases the DOS through LSM and enhances the corrosion and cavitation resistance by homogenizing surface composition. Due to the formation of a high-density surface and compressive residual stress along with grain refinement, it enhances the wear, hardness, and fatigue life of the materials, properties which determine the lifetimes of components. LST decreases the CoF by decreasing the reflectivity of light through texturing onto LST-treated solar panels to enhance efficiency.

(2) Ion beam treatment is a rapid, non-destructive, and low-temperature process that improves the mechanical and tribological properties and helps to down-select the materials for industrial equipment by fractography and failure analysis. HE of steel can be reduced by ion beam mixing. Ion implantation followed by ion deposition can increase hardness and reduce micro-cracks in high-speed tool steel. It is also used to make a protective coating that can reduce the oxidative degradation of spacecraft polymers.

(3) The surface properties of EB processes structural materials are far superior to its pre-treatment condition by processing under a controlled environment. It can also modify the surface properties of highly reactive materials, as the entire process occurs inside a vacuum environment.

(4) PIII uniformly implants ions on a complex 3D target to the desired concentration and depth, improving the mechanical and tribological properties of materials/components. PIII increases the lifespan of uranium metal and efficiently protects the Zr-cladding against HE, which limits hydrogen generation, significantly reducing the chance of accidents in nuclear power plants. It also enhances the wear and corrosion resist-

ance of the various components used in the oil & gas, aviation, and space industries. PIII was also used to develop a protective metal oxide coating over the satellites and spacecraft operating in LEO to prevent degradation of the components by reactive atomic oxygen.

(5) FSP, a novel solid-state surface engineering technology adapted from friction stir welding, deals with forming DRx fine-grain structures due to the extent of the plastic deformation. The fusion defects can easily be avoided, as the processing is performed under the melting temperature of the material. This allows microstructural changes of the processed region leading to significant enhancement of mechanical properties as compared to substrate materials.

**Acknowledgements** KKS acknowledges financial support from Uchchatar Avishkar Yojna organization. KKS and SM also acknowledge financial assistance from Naval Research Board, Defense Research and Development Organization. Doo-Man Chun and Sung-Tae Hong were supported by "Regional Innovation Strategy (RIS)" through the National Research Foundation of Korea (NRF) funded by the Ministry of Education (MOE) (2021RIS-003).

## Declarations

**Competing interests** The author(s) declare no competing interest.

## References

1. Morgan Stanley. (2020). Space: Investing in the Final Frontier. Retrieved November 5, 2022. https://www.morganstanley.com/ideas/investing-in-space.
2. International Civil Aviation Organization. (2019). Future of Aviation. Retrieved November 5, 2022. https://www.icao.int/Meetings/FutureOfAviation/Pages/default.aspx.
3. International Energy Agency. (2021). Oil 2021: Analysis and forecast to 2026. Retrieved November 5, 2022. https://www.iea.org/reports/oil-2021.
4. International Monetary Fund. (2021). World Economic Outlook: Managing Divergent Recoveries. Retrieved November 5, 2022. https://www.imf.org/en/Publications/WEO/Issues/2021/03/23/world-economic-outlook-april-2021.
5. International Atomic Energy Agency. (2019). IAEA Annual Report. Retrieved November 5, 2022. https://www.iaea.org/sites/default/files/publications/reports/2019/gc64-3.pdf.
6. NACE International. (2016). IMPACT (International Measures of Prevention, Application, and Economics of Corrosion Technologies Study) Report. Retrieved November 5, 2022. http://impact.nace.org/documents/Nace-International-Report.pdf.
7. Datta, T., Pathak, A. D., Basak, S., Gollapudi, S., & Sahu, K. K. (2021). Fractal behavior of surface oxide crack patterns on AISI 4140 high-strength low-alloy steel exposed to the simulated offshore environment. *Applied Surface Science Advances*. https://doi.org/10.1016/j.apsadv.2021.100110
8. Eliaz, N. (2019). Corrosion of metallic biomaterials: A review. *Materials, 12*(3), 407. https://doi.org/10.3390/ma12030407
9. Lim, D. W., Kim, J. H., Kim, B. C., Park, J. Y., & Ha, S. J. (2021). Evaluation of surface characteristics with pre-treatment polishing process in pulsed laser polishing AISI 4140 mold steel. *International Journal of Precision Engineering and Manufacturing, 22*, 1911–1921. https://doi.org/10.1007/s12541-021-00578-y
10. Gharari, R., Kazeminejad, H., Kojouri, N. M., & Hedayat, A. (2018). A review on hydrogen generation, explosion, and mitigation during severe accidents in light water nuclear reactors. *International Journal of Hydrogen Energy, 43*(4), 1939–1965. https://doi.org/10.1016/j.ijhydene.2017.11.174
11. Cakir, E., Sevgili, C., & Fiskin, R. (2021). An analysis of severity of oil spill caused by vessel accidents. *Transportation Research Part D: Transport and Environment, 90*, 102662. https://doi.org/10.1016/j.trd.2020.102662
12. Chen, J., Zhang, W., Li, S., Zhang, F., Zhu, Y., & Huang, X. (2018). Identifying critical factors of oil spill in the tanker shipping industry worldwide. *Journal of Cleaner Production, 180*, 1–10. https://doi.org/10.1016/j.jclepro.2017.12.238
13. Kwon, W., Kim, T., & Song, K. Y. (2021). Experimental investigation on $CO_2$ laser-assisted micro-grinding characteristics of $Al_2O_3$. *International Journal of Precision Engineering and Manufacturing, 22*, 51–62. https://doi.org/10.1007/s12541-020-00446-1
14. Barshilia, H. C. (2021). Surface modification technologies for aerospace and engineering applications: Current trends, challenges and future prospects. *Transactions of the Indian National Academy of Engineering, 6*(2), 173–188. https://doi.org/10.1007/s41403-021-00208-z
15. Allen, T., Busby, J., Meyer, M., & Petti, D. (2010). Materials challenges for nuclear systems. *Materials Today, 13*(12), 14–23. https://doi.org/10.1016/S1369-7021(10)70220-0
16. Martin, T. L., Coe, C., Bagot, P. A. J., Morrall, P., Smith, G. D. W., Scott, T., & Moody, M. P. (2016). Atomic-scale studies of uranium oxidation and corrosion by water vapour. *Scientific Reports, 6*(1), 1–10. https://doi.org/10.1038/srep25618
17. Krishnan, R. M. K. A., & Asundi, M. K. (1981). Zirconium alloys in nuclear technology. *Proceedings of the Indian Academy of Sciences Section C: Engineering Sciences, 4*(1), 41–56. https://doi.org/10.1007/BF02843474
18. Yagnik, S., & Garde, A. (2019). Zirconium alloys for LWR fuel cladding and core internals. *Structural Alloys for Nuclear Energy Applications*. https://doi.org/10.1016/B978-0-12-397046-6.00007-1
19. Hanawa, T. (2019). Overview of metals and applications. In *Metals for Biomedical Devices*, 3–29. Woodhead Publishing. https://doi.org/10.1016/B978-0-08-102666-3.00001-8.
20. Luiz, L. A., Kurelo, B. C. E. S., de Souza, G. B., de Andrade, J., & Marino, C. E. B. (2021). Effect of nitrogen plasma immersion ion implantation on the corrosion protection mechanisms of different stainless steels. *Materials Today Communications, 28*, 102655. https://doi.org/10.1016/j.mtcomm.2021.102655
21. Bharatiya, U., Gal, P., Agrawal, A., Shah, M., & Sircar, A. (2019). Effect of corrosion on crude oil and natural gas pipeline with emphasis on prevention by ecofriendly corrosion inhibitors: A comprehensive review. *Journal of Bio-and Tribo-Corrosion, 5*(2), 1–12. https://doi.org/10.1007/s40735-019-0225-9
22. Kermani, M. B., & Harrop, D. (1996). The impact of corrosion on the oil and gas industry. *SPE Production & Facilities, 11*(03), 186–190. https://doi.org/10.2118/29784-PA
23. Aglietti, G. S. (2020). Current challenges and opportunities for space technologies. *Frontiers in Space Technologies*. https://doi.org/10.3389/frspt.2020.00001
24. Froes, F., Boyer, R., & Dutta, B. (2019). Introduction to aerospace materials requirements and the role of additive manufacturing. In *Additive Manufacturing for the Aerospace Industry*, 1–6. Elsevier.

25. Mouritz, A. P. (2012). Fatigue of aerospace materials. In A.P. Mouritz (Ed.), *Introduction to Aerospace Materials* (1st ed., pp. 469–497). Woodhead Publishing.
26. Zhang, X., Chen, Y., & Hu, J. (2018). Recent advances in the development of aerospace materials. *Progress in Aerospace Sciences, 97*, 22–34. https://doi.org/10.1016/j.paerosci.2018.01.001
27. Wang, S. Y., Chu, P. K., Tang, B. Y., Zeng, X. C., & Wang, X. F. (1997). Improvement of the corrosion property of Cr4Mo4V bearing steel using plasma immersion ion implantation. *Nuclear Instruments and Methods in Physics Research Section B: Beam Interactions with Materials and Atoms, 127*, 1000–1003. https://doi.org/10.1016/S0168-583X(97)00047-5
28. Sankaran, K. K., & Mishra, R. S. (2017). Magnesium Alloys. In K. K. Sankaran and R. S. Mishra (Eds.), *Metallurgy and Design of Alloys with Hierarchical Microstructures* (1st ed., pp. 345–383). Elsevier.
29. Ueda, M., Dallaqua, R. S., Rossi, J. O., Tan, I. H., Abramof, E., Beloto, A. F., & Del Bosco, E. (2001). Metal-arc-plasma ion implantation of materials used in aerospace applications. In *PPPS-2001 Pulsed Power Plasma Science 2001. 28th IEEE International Conference on Plasma Science and 13th IEEE International Pulsed Power Conference. Digest of Papers (Cat. No. 01CH37251)*, 2, 1814–1817. IEEE. https://doi.org/10.1109/PPPS.2001.1001926.
30. Ueda, M., Tan, I. H., Dallaqua, R. S., Rossi, J. O., Barroso, J. J., & Tabacniks, M. H. (2003). Aluminum plasma immersion ion implantation in polymers. *Nuclear Instruments and Methods in Physics Research Section B: Beam Interactions with Materials and Atoms, 206*, 760–766. https://doi.org/10.1016/S0168-583X(03)00844-9
31. Tan, H., Ueda, M., Kostov, K., Nascente, P. A. P., & Demarquette, N. R. (2004). Polymer treatment by plasma immersion ion implantation of nitrogen for formation of diamond-like carbon film. *Japanese journal of applied physics, 43*(9R), 6399–6404. https://doi.org/10.1143/JJAP.43.6399
32. Tan, I. H., Ueda, M., Dallaqua, R. S., Rossi, J. O., Beloto, A. F., Tabacniks, M. H., Demarquette, N. R., & Inoue, Y. (2004). Treatment of polymers by plasma immersion ion implantation for space applications. *Surface and Coatings Technology, 186*(1–2), 234–238. https://doi.org/10.1016/j.surfcoat.2004.04.029
33. Dever, J., Banks, B., de Groh, K., & Miller, S. (2005). Degradation of spacecraft materials. In M. Kutz, (Ed.), *Handbook of environmental degradation of materials* (1st ed., pp. 465–501). William Andrew Publishing. https://doi.org/10.1557/mrs2010.612.
34. Sugioka, K., Meunier, M., & Piqué, A. (Eds.). (2010). Laser precision microfabrication (Vol. 135). Springer.
35. Yamamuro, Y., Shimoyama, T., & Yan, J. (2022). Microscale surface patterning of zirconia by femtosecond pulsed laser irradiation. *International Journal of Precision Engineering and Manufacturing-Green Technology, 9*(2), 619–632. https://doi.org/10.1007/s40684-021-00362-3
36. Draper, C. W., & Poate, J. M. (1985). Laser surface alloying. *International Metals Reviews, 30*(1), 85–108. https://doi.org/10.1179/imtr.1985.30.1.85
37. Lv, Y., Lei, L., Sun, L., & Cui, B. (2023). Improvement of the wear resistance of 20CrMnTi steel gear by discrete laser surface melting. *Optics & Laser Technology, 165*, 109598. https://doi.org/10.1016/j.optlastec.2023.109598
38. Hashemi, S. H., Mousavi, S. A., Razavi, R. S., Nourollahi, A., & Ashrafi, A. (2023). Laser surface melting of Al–Co–rare earth (Ce–La) alloys for improving corrosion resistance. *Optics & Laser Technology, 162*, 109256. https://doi.org/10.1016/j.optlastec.2023.109256
39. Yeo, H., Son, M., & Ki, H. (2022). Investigation of microstructure and residual stress development during laser surface melting of AH36 steel using 3-D fully coupled numerical model. *International Journal of Heat and Mass Transfer, 197*, 123366. https://doi.org/10.1016/j.ijheatmasstransfer.2022.123366
40. Yu, L., Bai, Y., Bian, T., Qu, Y., Xu, Z., Li, Y., & Zhang, H. (2023). Influence of laser parameters on corrosion resistance of laser melting layer on C45E4 steel surface. *Journal of Manufacturing Processes, 91*, 1–9. https://doi.org/10.1016/j.jmapro.2023.02.029
41. Jeyaprakash, N., Yang, C. H., & Kumar, D. R. (2020). Laser Surface Modification of Materials. In D. Yang (Ed.), *Practical Applications of Laser Ablation* (1st ed., pp. 61–81). IntechOpen.
42. Huang, W., Gao, X., Huang, Y., & Zhang, Y. (2023). Improved convolutional neural network for laser welding defect prediction. *International Journal of Precision Engineering and Manufacturing, 24*, 33–41. https://doi.org/10.1007/s12541-022-00729-9
43. Chaurasia, J. K., Jinoop, A. N., Parthasarathy, P., Paul, C. P., Bindra, K. S., & Bontha, S. (2021). Study of melt pool geometry and solidification microstructure during laser surface melting of Inconel 625 alloy. *Optik, 246*, 167766. https://doi.org/10.1016/j.ijleo.2021.167766
44. Ajmal, T. S., Arya, S. B., Maurya, P., & Shariff, S. M. (2022). Effect of hydrodynamics and laser surface melting on erosion-corrosion of X70 steel pipe elbow in oilfield slurry. *International Journal of Pressure Vessels and Piping, 199*, 104687. https://doi.org/10.1016/j.ijpvp.2022.104687
45. Jiao, Y., Brousseau, E., Kosai, K., Lunt, A. J., Yan, J., Han, Q., Zhu, H., Bigot, S., & He, W. (2021). Softening and hardening on a Zr-based bulk metallic glass induced by nanosecond laser surface melting. *Materials Science and Engineering: A, 803*, 140497. https://doi.org/10.1016/j.msea.2020.140497
46. Liu, R., Yu, J., Yang, Q., Wu, J., & Gao, S. (2021). Mechanical property and strengthening mechanism on DH36 marine steel after laser surface melting. *Surface and Coatings Technology, 425*, 127733. https://doi.org/10.1016/j.surfcoat.2021.127733
47. Hashim, M., & Duraiselvam, M. (2015). Enhancing tribological and corrosion resistance of Hastelloy C-276 through laser surface treatment. In P.R. Narayanan & S.V.S. Narayana Murty (Eds.), *Materials Science Forum* (Vol. 830, pp. 659–662). Trans Tech Publications Ltd.
48. Cui, Y. (2018). Influence of laser surface melting on tribological behaviour of AZ31B. *Surface Engineering, 34*(4), 296–300. https://doi.org/10.1080/02670844.2016.1246994
49. Charee, W., & Tangwarodomnukun, V. (2019). Experimental investigation and modeling of laser surface melting process for AISI 9254 commercially high silicon spring steel. *Optics & Laser Technology, 115*, 109–117. https://doi.org/10.1016/j.optlastec.2019.02.013
50. Shivakoti, I., Kibria, G., Cep, R., Pradhan, B. B., & Sharma, A. (2021). Laser surface texturing for biomedical applications: A review. *Coatings, 11*(2), 124. https://doi.org/10.3390/coatings11020124
51. Balamurugan, K. G. (2023). Effect of laser surface texturing parameters on the texture formation in pure magnesium substrate. *Materials Today: Proceedings, 72*, 2096–2101. https://doi.org/10.1016/j.matpr.2022.08.216
52. Caraguay, S. J., Pereira, T. S., Giacomelli, R. O., Cunha, A., Pereira, M., & Xavier, F. A. (2022). The effect of laser surface textures on the corrosion resistance of epoxy coated steel exposed to aggressive environments for offshore applications. *Surface and Coatings Technology, 437*, 128371. https://doi.org/10.1016/j.surfcoat.2022.128371
53. Sirdeshmukh, N., & Dongre, G. (2023). Achieving controlled topography and wettability through laser surface texturing of Ti6Al4V for bioengineering applications. *Results in Engineering, 17*, 100898. https://doi.org/10.1016/j.rineng.2023.100898
54. Cuao-Moreu, C. A., Campos-Silva, I., Delgado-Brito, A. M., Garcia-Sanchez, E. O., Juarez-Hernandez, A., Diabb-Zavala, J.

M., & Hernandez-Rodriguez, M. A. L. (2023). Effect of laser surface texturing and boriding on the tribocorrosion resistance of an ASTM F-1537 cobalt alloy. *Wear, 523*, 204799. https://doi.org/10.1016/j.wear.2023.204799
55. Liu, H., Tong, Z., Gu, J., Liu, C., Wang, X., & Ren, X. (2022). Effect of laser surface texturing depth and pattern on the bond strength and corrosion performance of phosphate conversion coating on magnesium alloy. *Optics & Laser Technology, 153*, 108164. https://doi.org/10.1016/j.optlastec.2022.108164
56. Riveiro, A., Maçon, A. L., del Val, J., Comesaña, R., & Pou, J. (2018). Laser surface texturing of polymers for biomedical applications. *Frontiers in physics, 6*, 16. https://doi.org/10.3389/fphy.2018.00016
57. Han, J., Zhang, F., Van Meerbeek, B., Vleugels, J., Braem, A., & Castagne, S. (2021). Laser surface texturing of zirconia-based ceramics for dental applications: A review. *Materials Science and Engineering: C, 123*, 112034. https://doi.org/10.1016/j.msec.2021.112034
58. Tong, W., & Xiong, D. (2022). Direct laser texturing technique for metal surfaces to achieve superhydrophobicity. *Materials Today Physics*. https://doi.org/10.1016/j.mtphys.2022.100651
59. Zabila, Y., Perzanowski, M., Dobrowolska, A., Kąc, M., Polit, A., & Marszałek, M. (2009). Direct laser interference patterning: Theory and application. *Acta Physica Polonica A, 115*(2), 591–593.
60. Mao, B., Siddaiah, A., Liao, Y., & Menezes, P. L. (2020). Laser surface texturing and related techniques for enhancing tribological performance of engineering materials: A review. *Journal of Manufacturing Processes, 53*, 153–173. https://doi.org/10.1016/j.jmapro.2020.02.009
61. Goldberg, P., Hariharan, A., Schell, F., Hantusch, M., Cichocka, M. O., Pérez, N., Voß, A., Giebeler, L., Hoffmann, V., Zwahr, C., Lasagni, A. F., & Gebert, A. (2023). Fine-tuning effect of direct laser interference patterning on the surface states and the corrosion behavior of a biomedical additively manufactured beta Ti alloy. *Corrosion Science*. https://doi.org/10.1016/j.corsci.2023.111230
62. Chen, J., Sabau, A. S., Meyer, H., III., & Leonard, D. (2021). Surface and subsurface characterization of laser-interference structured Ti6Al4V. *Applied Surface Science, 555*, 149576. https://doi.org/10.1016/j.apsusc.2021.149576
63. Schell, F., Alamri, S., Steege, T., Zwahr, C., Kunze, T., & Lasagni, A. (2022). On the wetting behavior of laser-microtextured stainless steel using direct laser interference patterning. *Surface and Coatings Technology, 447*, 128869. https://doi.org/10.1016/j.surfcoat.2022.128869
64. Wang, W., Boneberg, J., & Schmidt-Mende, L. (2021). Performance enhancement in Sb2S3 solar cell processed with direct laser interference patterning. *Solar Energy Materials and Solar Cells, 230*, 111235. https://doi.org/10.1016/j.solmat.2021.111235
65. Baumann, R., Milles, S., Leupolt, B., Kleber, S., Dahms, J., & Lasagni, A. F. (2021). Tailored wetting of copper using precise nanosecond direct laser interference patterning. *Optics and Lasers in Engineering, 137*, 106364. https://doi.org/10.1016/j.optlaseng.2020.106364
66. Mücklich, F., Lasagni, A., & Daniel, C. (2005). Laser interference metallurgy—periodic surface patterning and formation of intermetallics. *Intermetallics, 13*(3–4), 437–442. https://doi.org/10.1016/j.intermet.2004.07.005
67. Lu, C., & Lipson, R. H. (2010). Interference lithography: A powerful tool for fabricating periodic structures. *Laser & Photonics Reviews, 4*(4), 568–580. https://doi.org/10.1002/lpor.200810061
68. Wang, Y. R., Han, I. S., Jin, C. Y., & Hopkinson, M. (2020). Precise arrays of epitaxial quantum dots nucleated by in situ laser interference for quantum information technology applications. *ACS applied nano materials, 3*(5), 4739–4746. https://doi.org/10.1021/acsanm.0c00738
69. Mao, B., Liao, Y., & Li, B. (2018). Gradient twinning microstructure generated by laser shock peening in an AZ31B magnesium alloy. *Applied Surface Science, 457*, 342–351. https://doi.org/10.1016/j.apsusc.2018.06.176
70. Kuo, C., Chang, T., Liu, J., & Chung, C. (2021). Design, analytical and experimental evaluations of additive manufacturing for laser melting of polymer-metal colloids. *International Journal of Precision Engineering and Manufacturing, 22*, 1081–1096. https://doi.org/10.1007/s12541-021-00518-w
71. Lin, C., Wu, H., Li, Z., Yu, L., Zeng, J., Xia, C., Liao, Y., Xu, H., & Zhang, Y. (2022). Evaluation of oblique laser shock peening effect of FGH95 superalloy turbine disk material. *Materials Today Communications, 31*, 103534. https://doi.org/10.1016/j.mtcomm.2022.103534
72. Pan, X., Zhou, L., Wang, C., Yu, K., Zhu, Y., Yi, M., Wang, L., Wen, S., He, W., & Liang, X. (2023). Microstructure and residual stress modulation of 7075 aluminum alloy for improving fatigue performance by laser shock peening. *International Journal of Machine Tools and Manufacture, 184*, 103979. https://doi.org/10.1016/j.ijmachtools.2022.103979
73. Qin, R., Zhang, Z., Hu, Z., Du, Z., Xiang, X., Wen, G., & He, W. (2022). On-line evaluation and monitoring technology for material surface integrity in laser shock peening-A review. *Journal of Materials Processing Technology*. https://doi.org/10.1016/j.jmatprotec.2022.117851
74. Wang, W., Kattoura, M., Bovid, S., Zhang, Z., Lahrman, D., & Cai, W. (2023). Effects of nanosecond laser shock peening on residual stress, corrosion and tribocorrosion behavior of WE43 magnesium alloys. *Wear, 524*, 204866. https://doi.org/10.1016/j.wear.2023.204866
75. Dwivedi, P. K., Vinjamuri, R., Rai, A. K., Ganesh, P., Ranganathan, K., Bindra, K. S., & Dutta, K. (2022). Effect of laser shock peening on ratcheting strain accumulation, fatigue life and bulk texture evolution in HSLA steel. *International Journal of Fatigue, 163*, 107033. https://doi.org/10.1016/j.ijfatigue.2022.107033
76. Zhang, C., Dong, Y., & Ye, C. (2021). Recent developments and novel applications of laser shock peening: A review. *Advanced Engineering Materials, 23*(7), 2001216. https://doi.org/10.1002/adem.202001216
77. Yeo, I., Bae, S., Amanov, A., & Jeong, S. (2021). Effect of laser shock peening on properties of heat-treated Ti–6Al–4V manufactured by laser powder bed fusion. *International Journal of Precision Engineering and Manufacturing-Green Technology, 8*, 1137–1150. https://doi.org/10.1007/s40684-020-00234-2
78. Maleki, E., Bagherifard, S., Unal, O., Bandini, M., & Guagliano, M. (2022). On the effects of laser shock peening on fatigue behavior of V-notched AlSi10Mg manufactured by laser powder bed fusion. *International Journal of Fatigue, 163*, 107035. https://doi.org/10.1016/j.ijfatigue.2022.107035
79. Wu, J., Li, Y., Qiao, H., Yang, Y., Zhao, J., & Huang, Z. (2023). Prediction of mechanical properties and surface roughness of FGH4095 superalloy treated by laser shock peening based on XGBoost. *Journal of Alloys and Metallurgical Systems, 1*, 100001. https://doi.org/10.1016/j.jalmes.2023.100001
80. Azevedo, L., Kashaev, N., Horstmann, C., Ventzke, V., Furtado, C., Moreira, P. M., & Tavares, P. J. (2022). Fatigue behaviour of laser shock peened AISI D2 tool steel. *International Journal of Fatigue, 165*, 107226. https://doi.org/10.1016/j.ijfatigue.2022.107226
81. Yang, Y., Lu, Y., Shi, W., Hou, B., Qiao, H., Qi, J., Zhang, E., & Qin, G. (2023). Improvement of biocorrosion resistance and antibacterial performance of Ti–3Tu alloy subjected to laser shock

peening. *Optics & Laser Technology, 158*, 108794. https://doi.org/10.1016/j.optlastec.2022.108794
82. Kumar, R. R., Devasena, T., & Abeens, M. (2023). Improved mechanical properties of nano structured 316 L stainless steel by statistically optimized low pulsed laser shock peening process for aeronautical application. *Optik, 276*, 170654. https://doi.org/10.1016/j.ijleo.2023.170654
83. Pan, X., Guo, S., Tian, Z., Liu, P., Dou, L., Wang, X., An, Z., & Zhou, L. (2021). Fatigue performance improvement of laser shock peened hole on powder metallurgy Ni-based superalloy labyrinth disc. *Surface and Coatings Technology, 409*, 126829. https://doi.org/10.1016/j.surfcoat.2021.126829
84. Mao, B., Liao, Y., & Li, B. (2019). Abnormal twin-twin interaction in an Mg-3Al-1Zn magnesium alloy processed by laser shock peening. *Scripta Materialia, 165*, 89–93. https://doi.org/10.1016/j.scriptamat.2019.02.028
85. Ezhilmaran, V., Vijayaraghavan, L., & Vasa, N. J. (2017). Investigation of Nd3+: YAG laser aided surface texturing to improve tribological characteristics of piston ring. *Journal of Laser Micro Nanoengineering, 12*(3), 195–202.
86. Bathe, R., Sai Krishna, V., Nikumb, S. K., & Padmanabham, G. J. A. P. A. (2014). Laser surface texturing of gray cast iron for improving tribological behavior. *Applied Physics A, 117*(1), 117–123. https://doi.org/10.1007/s00339-014-8281-y
87. Yang, L., Ding, Y., Cheng, B., He, J., Wang, G., & Wang, Y. (2018). Investigations on femtosecond laser modified microtextured surface with anti-friction property on bearing steel GCr15. *Applied Surface Science, 434*, 831–842. https://doi.org/10.1016/j.apsusc.2017.10.234
88. Lin, J., Chen, F., Tang, X., Liu, J., Shen, S., & Ge, G. (2020). Radiation-induced swelling and hardening of 316L stainless steel fabricated by selected laser melting. *Vacuum, 174*, 109183. https://doi.org/10.1016/j.vacuum.2020.109183
89. De Damborena, J., Vazquez, A. J., Gonzalez, J. A., & West, D. R. F. (1989). Elimination of intergranular corrosion susceptibility of a sensitised 304 steel by subsequent laser surface melting. *Surface Engineering, 5*(3), 235–238. https://doi.org/10.1179/sur.1989.5.3.235
90. Kwok, C. T., Lo, K. H., Chan, W. K., Cheng, F. T., & Man, H. C. (2011). Effect of laser surface melting on intergranular corrosion behaviour of aged austenitic and duplex stainless steels. *Corrosion Science, 53*(4), 1581–1591. https://doi.org/10.1016/j.corsci.2011.01.048
91. Lim, Y. S., Kim, H. P., Han, J. H., Kim, J. S., & Kwon, H. S. (2001). Influence of laser surface melting on the susceptibility to intergranular corrosion of sensitized Alloy 600. *Corrosion science, 43*(7), 1321–1335. https://doi.org/10.1016/S0010-938X(00)00149-9
92. Pacquentin, W., Gouton, L., Caron, N., Brussieux, C., Foucault, M., Peyre, P., Maskrot, H., & Favier, V. (2021). Laser surface melting of nickel-based alloy reduces nickel release in the primary cooling system of a nuclear power plant. *Optics & Laser Technology, 144*, 107401. https://doi.org/10.1016/j.optlastec.2021.107401
93. Hashim, M., Babu, K. S. R., Duraiselvam, M., & Natu, H. (2013). Improvement of wear resistance of Hastelloy C-276 through laser surface melting. *Materials & Design, 46*, 546–551. https://doi.org/10.1016/j.matdes.2012.10.024
94. Tang, C. H., Cheng, F. T., & Man, H. C. (2004). Improvement in cavitation erosion resistance of a copper-based propeller alloy by laser surface melting. *Surface and Coatings Technology, 182*(2–3), 300–307. https://doi.org/10.1016/j.surfcoat.2003.08.048
95. Cottam, R., Luzin, V., Moody, H., Edwards, D., Majumdar, A., Wong, Y. C., Wang, J., & Brandt, M. (2014). The role of microstructural characteristics in the cavitation erosion behaviour of laser melted and laser processed Nickel–Aluminium Bronze. *Wear, 317*(1–2), 56–63. https://doi.org/10.1016/j.wear.2014.05.002
96. Kwok, C. T., Man, H. C., & Cheng, F. T. (2000). Cavitation erosion and pitting corrosion behaviour of laser surface-melted martensitic stainless steel UNS S42000. *Surface and Coatings Technology, 126*(2–3), 238–255. https://doi.org/10.1016/S0257-8972(00)00533-8
97. Singh, A., & Harimkar, S. P. (2012). Laser surface engineering of magnesium alloys: A review. *JOM Journal of the Minerals Metals and Materials Society, 64*(6), 716–733. https://doi.org/10.1007/s11837-012-0340-2
98. Abbas, G., Liu, Z., & Skeldon, P. (2005). Corrosion behaviour of laser-melted magnesium alloys. *Applied Surface Science, 247*(1–4), 347–353. https://doi.org/10.1016/j.apsusc.2005.01.169
99. Abbas, G., Li, L., Ghazanfar, U., & Liu, Z. (2006). Effect of high power diode laser surface melting on wear resistance of magnesium alloys. *Wear, 260*(1–2), 175–180. https://doi.org/10.1016/j.wear.2005.01.036
100. Majumdar, J. D., Galun, R., Mordike, B. L., & Manna, I. (2003). Effect of laser surface melting on corrosion and wear resistance of a commercial magnesium alloy. *Materials Science and Engineering: A, 361*(1–2), 119–129. https://doi.org/10.1016/S0921-5093(03)00519-7
101. Mondal, A. K., Kumar, S., Blawert, C., & Dahotre, N. B. (2008). Effect of laser surface treatment on corrosion and wear resistance of ACM720 Mg alloy. *Surface and Coatings Technology, 202*(14), 3187–3198. https://doi.org/10.1016/j.surfcoat.2007.11.030
102. Tian, Y. S., Chen, C. Z., Li, S. T., & Huo, Q. H. (2005). Research progress on laser surface modification of titanium alloys. *Applied surface science, 242*(1–2), 177–184. https://doi.org/10.1016/j.apsusc.2004.08.011
103. Langlade, C., Vannes, A. B., Krafft, J. M., & Martin, J. R. (1998). Surface modification and tribological behaviour of titanium and titanium alloys after YAG-laser treatments. *Surface and Coatings Technology, 100*, 383–387. https://doi.org/10.1016/S0257-8972(97)00653-1
104. Yue, T. M., Yu, J. K., Mei, Z., & Man, H. C. (2002). Excimer laser surface treatment of Ti–6Al–4V alloy for corrosion resistance enhancement. *Materials Letters, 52*(3), 206–212. https://doi.org/10.1016/S0167-577X(01)00395-0
105. Ardila-Rodríguez, L. A., Menezes, B. R. C., Pereira, L. A., Takahashi, R. J., Oliveira, A. C., & Travessa, D. N. (2019). Surface modification of aluminum alloys with carbon nanotubes by laser surface melting. *Surface and Coatings Technology, 377*, 124930. https://doi.org/10.1016/j.surfcoat.2019.124930
106. Etsion, I. (2005). State of the art in laser surface texturing. *Journal of Tribology, 127*(1), 248–253. https://doi.org/10.1115/1.1828070
107. Li, X., Li, Y., Tong, Z., Ma, Q., Ni, Y., & Dong, G. (2019). Enhanced lubrication effect of gallium-based liquid metal with laser textured surface. *Tribology International, 129*, 407–415. https://doi.org/10.1016/j.triboint.2018.08.037
108. Sasi, R., Subbu, S. K., & Palani, I. A. (2017). Performance of laser surface textured high speed steel cutting tool in machining of Al7075-T6 aerospace alloy. *Surface and Coatings Technology, 313*, 337–346. https://doi.org/10.1016/j.surfcoat.2017.01.118
109. Ta, D. V., Dunn, A., Wasley, T. J., Kay, R. W., Stringer, J., Smith, P. J., Connaughton, C., & Shephard, J. D. (2015). Nanosecond laser textured superhydrophobic metallic surfaces and their chemical sensing applications. *Applied Surface Science, 357*, 248–254. https://doi.org/10.1016/j.apsusc.2015.09.027
110. Ijaola, A. O., Bamidele, E. A., Akisin, C. J., Bello, I. T., Oyatobo, A. T., Abdulkareem, A., Farayibi, P. K., & Asmatulu, E. (2020). Wettability transition for laser textured surfaces: A

comprehensive review. *Surfaces and Interfaces, 21*, 100802. https://doi.org/10.1016/j.surfin.2020.100802
111. Yang, H., Sun, K., Xue, Y., Xu, C., Fan, D., Cao, Y., & Xue, W. (2019). Controllable drop splashing on picosecond laser patterned hybrid superhydrophobic/-philic surfaces. *Applied Surface Science, 481*, 184–191. https://doi.org/10.1016/j.apsusc.2019.02.241
112. Sun, K., Yang, H., Xue, W., He, A., Zhu, D., Liu, W., Adeyemi, K., & Cao, Y. (2018). Anti-biofouling superhydrophobic surface fabricated by picosecond laser texturing of stainless steel. *Applied Surface Science, 436*, 263–267. https://doi.org/10.1016/j.apsusc.2017.12.012
113. Tong, Z., Pan, X., Zhou, W., Yang, Y., Ye, Y., Qian, D., & Ren, X. (2021). Achieving excellent wear and corrosion properties in laser additive manufactured CrMnFeCoNi high-entropy alloy by laser shock peening. *Surface and Coatings Technology, 422*, 127504. https://doi.org/10.1016/j.surfcoat.2021.127504
114. Sher, M. J., Winkler, M. T., & Mazur, E. (2011). Pulsed-laser hyperdoping and surface texturing for photovoltaics. *MRS Bulletin, 36*(6), 439–445. https://doi.org/10.1557/mrs.2011.111
115. Horn, A., Kalmbach, C. C., Moreno, J. G., Schütz, V., Stute, U., & Overmeyer, L. (2012). Laser-surface-treatment for photovoltaic applications. *Physics Procedia, 39*, 709–716. https://doi.org/10.1016/j.phpro.2012.10.092
116. Pereira, D., Oliveira, J. P., Santos, T. G., Miranda, R. M., Lourenço, F., Gumpinger, J., & Bellarosa, R. (2019). Aluminium to carbon fibre reinforced polymer tubes joints produced by magnetic pulse welding. *Composite Structures, 230*, 111512. https://doi.org/10.1016/j.compstruct.2019.111512
117. Tan, C., Su, J., Feng, Z., Liu, Y., Chen, B., & Song, X. (2021). Laser joining of CFRTP to titanium alloy via laser surface texturing. *Chinese Journal of Aeronautics, 34*(5), 103–114. https://doi.org/10.1016/j.cja.2020.08.017
118. Ge, M. Z., & Xiang, J. Y. (2016). Effect of laser shock peening on microstructure and fatigue crack growth rate of AZ31B magnesium alloy. *Journal of Alloys and Compounds, 680*, 544–552. https://doi.org/10.1016/j.jallcom.2016.04.179
119. Jain, I. P., & Agarwal, G. (2011). Ion beam induced surface and interface engineering. *Surface Science Reports, 66*(3–4), 77–172. https://doi.org/10.1016/j.surfrep.2010.11.001
120. Bolse, W. (1998). Mechanisms of ion beam induced atomic mixing in solids. *Materials Science and Engineering: A, 253*(1–2), 194–201. https://doi.org/10.1016/S0921-5093(98)00727-8
121. Zhang, K., Lieb, K. P., Milinovic, V., Uhrmacher, M., & Klaumünzer, S. (2006). Interface mixing and magnetism in Ni/Si bilayers irradiated with swift and low-energy heavy ions. *Nuclear Instruments and Methods in Physics Research Section B: Beam Interactions with Materials and Atoms, 249*(1–2), 167–171. https://doi.org/10.1016/j.nimb.2006.03.106
122. Uchida, H., Yamashita, M., Hanaki, S., & Ueta, T. (2004). Characterization of (Ti, Al) N films prepared by ion mixing and vapor deposition. *Materials Science and Engineering: A, 387*, 758–762. https://doi.org/10.1016/j.msea.2004.03.096
123. Knutsson, A., Johansson, M. P., Karlsson, L., & Odén, M. (2011). Machining performance and decomposition of TiAlN/TiN multilayer coated metal cutting inserts. *Surface and Coatings Technology, 205*(16), 4005–4010. https://doi.org/10.1016/j.surfcoat.2011.02.031
124. Ensinger, W., Schröer, A., & Wolf, G. K. (1992). Are coatings produced by ion-beam-assisted deposition superior? A comparison of chemical and mechanical properties of steel coated using different deposition techniques. *Surface and Coatings Technology, 51*(1–3), 217–221. https://doi.org/10.1016/0257-8972(92)90241-2
125. Kussmaul, M., Mirtich, M. J., & Curren, A. (1992). Ion beam treatment of potential space materials at the NASA Lewis research center. *Surface and Coatings Technology, 51*(1–3), 299–306. https://doi.org/10.1016/0257-8972(92)90254-8
126. Pelaz, L., Marqués, L. A., & Barbolla, J. (2004). Ion-beam-induced amorphization and recrystallization in silicon. *Journal of Applied Physics, 96*(11), 5947–5976. https://doi.org/10.1063/1.1808484
127. Carter, G., & Nobes, M. J. (1991). A phenomenological model of ion-induced crystallization and amorphization. *Journal of Materials Research, 6*(10), 2103–2108. https://doi.org/10.1557/JMR.1991.2103
128. Larson, L. A., Williams, J. M., & Current, M. I. (2011). Ion implantation for semiconductor doping and materials modification. *Reviews of Accelerator Science and Technology*. https://doi.org/10.1142/9789814383998_0002
129. Thomé, L., & Garrido, F. (2001). Application of ion beams to nuclear waste issues: Evaluation of nuclear ceramics. *Vacuum, 63*(4), 619–626. https://doi.org/10.1016/S0042-207X(01)00250-0
130. Keller, L. M., Holzer, L., Wepf, R., Gasser, P., Münch, B., & Marschall, P. (2011). On the application of focused ion beam nanotomography in characterizing the 3D pore space geometry of Opalinus clay. *Physics and Chemistry of the Earth, Parts A/B/C, 36*(17–18), 1539–1544. https://doi.org/10.1016/j.pce.2011.07.010
131. Parada, M. A., Delalez, N., De Almeida, A., Muntele, C., Muntele, I., & Ila, D. (2006). Low energy ion beam induced changes in ETFE polymer. *Nuclear Instruments and Methods in Physics Research Section B: Beam Interactions with Materials and Atoms, 242*(1–2), 550–552. https://doi.org/10.1016/j.nimb.2005.08.147
132. Nastasi, M., Mayer, J. W., & Wang, Y. (2014). *Ion beam analysis: Fundamentals and applications*. CRC Press.
133. Redondo-Cubero, A., Borge, M. J. G., Gordillo, N., Gutiérrez, P. C., Olivares, J., Pérez Casero, R., & Ynsa, M. D. (2021). Current status and future developments of the ion beam facility at the centre of micro-analysis of materials in Madrid. *The European Physical Journal Plus, 136*, 1–16. https://doi.org/10.1140/epjp/s13360-021-01085-9
134. Sella, C., Lecoeur, J., Sampeur, Y., & Catania, P. (1993). Corrosion resistance of amorphous hydrogenated SiC and diamond-like coatings deposited by rf-plasma-enhanced chemical vapour deposition. *Surface and Coatings Technology, 60*(1–3), 577–583. https://doi.org/10.1016/0257-8972(93)90156-I
135. Park, J. W., Chun, Y., & Chang, J. (2007). Effects of ion beam mixing of silicon carbide film deposited onto metallic materials for application to nuclear hydrogen production. *Journal of Nuclear Materials, 362*(2–3), 268–273. https://doi.org/10.1016/j.jnucmat.2007.01.129
136. Allen, G. C., & Stevens, J. C. (1988). The behaviour of uranium metal in hydrogen atmospheres. *Journal of the Chemical Society, Faraday Transactions 1: Physical Chemistry in Condensed Phases., 84*(1), 165–174. https://doi.org/10.1039/F19888400165
137. Luo, L., Lai, X., & Wang, X. (2014). Recent advances in study of uranium surface chemistry in China. *Radiochimica Acta, 102*(1–2), 27–39. https://doi.org/10.1515/ract-2014-2124
138. Banos, A., Harker, N. J., & Scott, T. B. (2018). A review of uranium corrosion by hydrogen and the formation of uranium hydride. *Corrosion Science, 136*, 129–147. https://doi.org/10.1016/j.corsci.2018.03.002
139. Liang, W., Ling, Y., Liu, K., Hu, Y., Yin, A., Zhu, F., Chen, L., & Zhang, Z. (2018). Corrosion resistance and mechanism of CeN, TiN and CeN/TiN bilayer composite film deposited by dual ion beam sputtering. *Surface and Coatings Technology, 335*, 280–287. https://doi.org/10.1016/j.surfcoat.2017.12.033

140. Couland, M., Fourcaudot, S., Jovani Abril, R., Fernandez-Carretero, A., & Somers, J. (2012). Novel production route of yttria-stabilized zirconia fuel kernels and pellets for nuclear fuel applications. *Journal of the American Ceramic Society, 95*(1), 133–137. https://doi.org/10.1111/j.1551-2916.2011.04854.x
141. Zhang, Y., Zhao, Z., & Guo, G. (2017). Irradiation effects of displacement damage and gas atoms in Yttria stabilized zirconia irradiated by Au and helium ions. *Nuclear Instruments and Methods in Physics Research Section B: Beam Interactions with Materials and Atoms, 403*, 33–37. https://doi.org/10.1016/j.nimb.2017.04.092
142. Perez, T. E. (2013). Corrosion in the oil and gas industry: An increasing challenge for materials. *JOM Journal of the Minerals Metals and Materials Society, 65*(8), 1033–1042. https://doi.org/10.1007/s11837-013-0675-3
143. Cabrini, M., Lorenzi, S., Marcassoli, P., & Pastore, T. (2011). Hydrogen embrittlement behavior of HSLA line pipe steel under cathodic protection. *Corrosion Review, 29*(5–6), 261–274. https://doi.org/10.1515/CORRREV.2011.009
144. Rhodes, P. R. (2001). Environment-assisted cracking of corrosion-resistant alloys in oil and gas production environments: A review. *Corrosion, 57*(11), 923–966. https://doi.org/10.5006/1.3290320
145. Huang, W., Asmann, M., Cao, F., Srinivasan, R., Ma, N., Mueller, R., & Ayer, R. (2013, March). SSC resistance and cracking behavior of 125ksi grade low alloy OCTG in sour environments. In CORROSION 2013. OnePetro.
146. Chakrabarty, T., & Smith, R. J. (2012). Identification of SSC (Sulfide Stress Cracking)-Susceptible Wells and Risk Prediction. In *SPE Heavy Oil Conference Canada*. OnePetro. https://doi.org/10.2118/160489-MS
147. Hirth, J. P. (1980). Effects of hydrogen on the properties of iron and steel. *Metallurgical Transactions A, 11*(6), 861–890. https://doi.org/10.1007/BF02654700
148. Martin, M. L., Robertson, I. M., & Sofronis, P. (2011). Interpreting hydrogen-induced fracture surfaces in terms of deformation processes: A new approach. *Acta Materialia, 59*(9), 3680–3687. https://doi.org/10.1016/j.actamat.2011.03.002
149. Robertson, I. M., Sofronis, P., Nagao, A., Martin, M. L., Wang, S., Gross, D. W., & Nygren, K. E. (2015). Hydrogen embrittlement understood. *Metallurgical and Materials Transactions A, 46*(6), 2323–2341. https://doi.org/10.1007/s11661-015-2836-1
150. Nagumo, M. (2004). Hydrogen related failure of steels–a new aspect. *Materials Science and Technology, 20*(8), 940–950. https://doi.org/10.1179/026708304225019687
151. Nagumo, M. (2001). Function of hydrogen in embrittlement of high-strength steels. *ISIJ international, 41*(6), 590–598. https://doi.org/10.2355/isijinternational.41.590
152. Oriani, R. A. (1987). Whitney award lecture—1987: Hydrogen—the versatile embrittler. *Corrosion, 43*(7), 390–397. https://doi.org/10.5006/1.3583875
153. Gerberich, W. W., Oriani, R. A., Lji, M. J., Chen, X., & Foecke, T. (1991). The necessity of both plasticity and brittleness in the fracture thresholds of iron. *Philosophical Magazine A, 63*(2), 363–376. https://doi.org/10.1080/01418619108204854
154. Srinivasan, R., & Neeraj, T. (2014). Hydrogen embrittlement of ferritic steels: Deformation and failure mechanisms and challenges in the oil and gas industry. *JOM Journal of the Minerals Metals and Materials Society, 66*(8), 1377–1382. https://doi.org/10.1007/s11837-014-1054-4
155. Neeraj, T., Srinivasan, R., & Li, J. (2012). Hydrogen embrittlement of ferritic steels: Observations on deformation microstructure, nanoscale dimples and failure by nanovoiding. *Acta Materialia, 60*(13–14), 5160–5171. https://doi.org/10.1016/j.actamat.2012.06.014
156. Zucato, I., Moreira, M. C., Machado, I. F., & Lebrão, S. M. G. (2002). Microstructural characterization and the effect of phase transformations on toughness of the UNS S31803 duplex stainless steel aged treated at 850 °C. *Materials Research, 5*, 385–389. https://doi.org/10.1590/S1516-14392002000300026
157. Bruch, D., Henes, D., Leibenguth, P., & Holzapfel, C. (2008). Mechanichal properties and corrosion resistance of duplex stainless steel forgings with large wall thicknesses. *La Metallurgia Italiana*.
158. Wilde, B. E., Kim, C. D., & Turn, J. C., Jr. (1982). The influence of noble metal additions on the sulfide corrosion performance of AISI 4130 steel. *Corrosion, 38*(10), 515–524. https://doi.org/10.5006/1.3593854
159. Lumsden, J. B., Wilde, B. E., & Stocker, P. J. (1983). Effect of palladium additions to AISI 4130 steel on its sulfide cracking susceptibility. *Scripta metallurgica, 17*(8), 971–974. https://doi.org/10.1016/0036-9748(83)90432-5
160. Wilde, B. E., & Shimada, T. (1988). Surface modification: A potential new approach to combatting hydrogen induced fracture in steel. *Scripta metallurgica, 22*(4), 551–556. https://doi.org/10.1016/0036-9748(88)90023-3
161. Wilde, B. E., Chattoraj, I., & Mozhi, T. A. (1987). The influence of palladium on the resistance of low alloy steels to hydrogen embrittlement. *Scripta metallurgica, 21*(10), 1369–1373. https://doi.org/10.1016/0036-9748(87)90115-3
162. Edgar, J., & Tint, S. (2015). Additive manufacturing technologies: 3D printing, rapid prototyping, and direct digital manufacturing. *Johnson Matthey Technology Review, 59*(3), 193–198. https://doi.org/10.1595/205651315X688406
163. Vityaz, P. A., Kheifetz, M. L., & Chizhik, S. A. (2019). Synergetic technologies of direct layer deposition in aerospace additive manufacturing. In F. Froes & R. Boyer (Eds.), *Additive Manufacturing for the Aerospace Industry* (1st ed., pp. 427–447). Elsevier.
164. Gordienko, A. I., Kheifetz, M. L., Kozhouro, L. M., Rakomsin, A. P., Sidorenko, M. I., Eidelman, E. D., & Senchilo, I. A. (2004). Combined physico-chemical treatment: Synergetic aspect. *Minsk: Technoprint*.
165. Tang, C. B., Liu, D. X., Zhang, Q., & Zhang, X. H. (2011). Effect of Ti/Mo and Cr/Mo metallic multilayer films on fretting fatigue resistance of Ti–6Al–4V alloy. *Materials Research Innovations, 15*(sup1), s166–s170. https://doi.org/10.1179/143307511X12858956848038
166. Leger, L. J. (1982). Oxygen atom reaction with shuttle materials at orbital altitudes (No. S-516).
167. Miller, S. K., & Banks, B. (2010). Degradation of spacecraft materials in the space environment. *MRS bulletin, 35*(1), 20–24. https://doi.org/10.1557/mrs2010.612
168. Banks, B., Mirtich, M., Rutledge, S., Swec, D., & Nahra, H. (1985). Ion beam sputter-deposited thin film coatings for protection of spacecraft polymers in low earth orbit. In *23rd Aerospace Sciences Meeting*, p. 420. https://doi.org/10.2514/6.1985-420.
169. Kang, J. G., Kim, J. S., Min, B. K., & Kang, E. G. (2023). Inlet hole shape analysis depending on the focus conditions for electron beam micro-hole drilling. *International Journal of Precision Engineering and Manufacturing*. https://doi.org/10.1007/s12541-023-00785-9
170. Węglowski, M. S., Błacha, S., & Phillips, A. (2016). Electron beam welding–techniques and trends–review. *Vacuum, 130*, 72–92. https://doi.org/10.1016/j.vacuum.2016.05.004
171. Zou, J., Qin, Y., Dong, C., Wang, X., Wu, A., & Hao, S. (2004). Numerical simulation of the thermal-mechanical process of high current pulsed electron beam treatment. *Journal of Vacuum Science & Technology A: Vacuum, Surfaces, and Films, 22*(3), 545–552. https://doi.org/10.1116/1.1697481

172. Han, S. W., Yoo, H., Shin, S., Kim, H., Lee, G., Jeon, J., Han, S., & Cho, J. (2023). Parameter optimization of WAAM with pulsed GMAW for manufacturing propeller-shaped blade. *International Journal of Precision Engineering and Manufacturing, 24*, 1103–1110. https://doi.org/10.1007/s12541-023-00797-5
173. Zenker, R., Sacher, G., Buchwalder, A., Liebich, J., Reiter, A., & Häßler, R. (2007). Hybrid technology hard coating–electron beam surface hardening. *Surface and Coatings Technology, 202*(4–7), 804–808. https://doi.org/10.1016/j.surfcoat.2007.05.089
174. Valkov, S., Ormanova, M., & Petrov, P. (2020). Electron-beam surface treatment of metals and alloys: Techniques and trends. *Metals, 10*(9), 1219. https://doi.org/10.3390/met10091219
175. Wahlmann, B., Körner, C., & Nunn, M. (2021). Electron beam wire cladding of nickel alloys and stainless steel on a reactor pressure vessel steel. *Materials Science and Engineering: A, 811*, 141082. https://doi.org/10.1016/j.msea.2021.141082
176. Hao, S., & Li, M. (2016). Producing nano-grained and Al-enriched surface microstructure on AZ91 magnesium alloy by high current pulsed electron beam treatment. *Nuclear Instruments and Methods in Physics Research Section B: Beam Interactions with Materials and Atoms, 375*, 1–4. https://doi.org/10.1016/j.nimb.2016.03.035
177. Walker, J. C., Murray, J. W., Nie, M., Cook, R. B., & Clare, A. T. (2014). The effect of large-area pulsed electron beam melting on the corrosion and microstructure of a Ti6Al4V alloy. *Applied Surface Science, 311*, 534–540. https://doi.org/10.1016/j.apsusc.2014.05.105
178. Gao, Y. K. (2013). Influence of pulsed electron beam treatment on microstructure and properties of TA15 titanium alloy. *Applied Surface Science, 264*, 633–635. https://doi.org/10.1016/j.apsusc.2012.10.083
179. Zagulyaev, D., Konovalov, S., Gromov, V., Glezer, A., Ivanov, Y., & Sundeev, R. (2018). Structure and properties changes of Al-Si alloy treated by pulsed electron beam. *Materials Letters, 229*, 377–380. https://doi.org/10.1016/j.matlet.2018.07.064
180. Guo, G., Tang, G., Ma, X., Sun, M., & Ozur, G. E. (2013). Effect of high current pulsed electron beam irradiation on wear and corrosion resistance of Ti6Al4V. *Surface and Coatings Technology, 229*, 140–145. https://doi.org/10.1016/j.surfcoat.2012.08.009
181. Basak, S., Sahu, K. K., Sharma, S. K., & Majumdar, J. D. (2017). Studies on electron beam surface melting of AISI 316 stainless steel and AISI 347 stainless steel. *Procedia Manufacturing, 7*, 647–653. https://doi.org/10.1016/j.promfg.2016.12.096
182. Basak, S., Sharma, S. K., Mondal, M., Sahu, K. K., Gollapudi, S., Dutta Majumdar, J., & Hong, S. T. (2021). Electron beam surface treatment of 316L austenitic stainless steel: improvements in hardness, wear, and corrosion resistance. *Metals and Materials International, 27*(5), 953–961. https://doi.org/10.1007/s12540-020-00773-y
183. Basak, S., Sharma, S. K., Sahu, K. K., Gollapudi, S., & Majumdar, J. D. (2019). Surface modification of structural material for nuclear applications by electron beam melting: Enhancement of microstructural and corrosion properties of Inconel 617. *SN Applied Sciences, 1*(7), 1–12. https://doi.org/10.1007/s42452-019-0744-5
184. Yang, J., Le, K., Chen, H., Zhao, X., Xie, X., Luo, Y., Xu, S., & Liu, W. (2023). The significantly enhanced mechanical and tribological performances of the dual plasma nitrided and PVD Coated Ti6Al4V alloy. *International Journal of Precision Engineering and Manufacturing, 24*, 607–609. https://doi.org/10.1007/s12541-023-00770-2
185. Conrad, J. R., Radtke, J. L., Dodd, R. A., Worzala, F. J., & Tran, N. C. (1987). Plasma source ion-implantation technique for surface modification of materials. *Journal of Applied Physics, 62*(11), 4591–4596. https://doi.org/10.1063/1.339055
186. Tendys, J., Donnelly, I. J., Kenny, M. J., & Pollock, J. T. A. (1988). Plasma immersion ion implantation using plasmas generated by radio frequency techniques. *Applied Physics Letters, 53*(22), 2143–2145. https://doi.org/10.1063/1.100299
187. Gupta, D. (2011). Plasma immersion ion implantation (PIII) process-physics and technology. *Int. J. Adv. Technol, 2*(4), 471–490.
188. Conrad, J. R., Dodd, R. A., Han, S., Madapura, M., Scheuer, J., Sridharan, K., & Worzala, F. J. (1990). Ion beam assisted coating and surface modification with plasma source ion implantation. *Journal of Vacuum Science & Technology A: Vacuum, Surfaces, and Films, 8*(4), 3146–3151. https://doi.org/10.1116/1.576598
189. Mantese, J. V., Brown, I. G., Cheung, N. W., & Collins, G. A. (1996). Plasma-immersion ion implantation. *Mrs Bulletin, 21*(8), 52–56. https://doi.org/10.1557/S0883769400035727
190. Blawert, C., & Mordike, B. L. (1997). Industrial applications of plasma immersion ion implantation. *Surface and Coatings Technology, 93*(2–3), 274–279. https://doi.org/10.1016/S0257-8972(97)00060-1
191. Kashkarov, E. B., Nikitenkov, N. N., Sutygina, A. N., Syrtanov, M. S., Vilkhivskaya, O. V., Pryamushko, T. S., Kudiiarov, V. N., & Volesky, L. (2016). Effect of titanium ion implantation and deposition on hydrogenation behavior of Zr-1Nb alloy. *Surface and Coatings Technology, 308*, 2–9. https://doi.org/10.1016/j.surfcoat.2016.07.111
192. Tian, X. B., Fu, K. Y., Chu, P. K., & Yang, S. Q. (2005). Plasma immersion ion implantation of insulating materials. *Surface and Coatings Technology, 196*(1–3), 162–166. https://doi.org/10.1016/j.surfcoat.2004.08.166
193. Ueda, M., Silva, C., Marcondes, A. R., Reuther, H., & De Souza, G. B. (2018). Recent experiments on plasma immersion ion implantation (and deposition) using discharges inside metal tubes. *Surface and Coatings Technology, 355*, 98–110. https://doi.org/10.1016/j.surfcoat.2018.05.009
194. Mariano, S. D. F. M., Ueda, M., Oliveira, R. M., Pillaca, E. J. D. D. M., & Dos Santos, N. M. (2017). Magnetic-field enhanced plasma immersion ion implantation and deposition (PIII&D) of diamond-like carbon films inside tubes. *Surface and Coatings Technology, 312*, 47–54. https://doi.org/10.1016/j.surfcoat.2016.08.077
195. Anders, A. (1997). Metal plasma immersion ion implantation and deposition: A review. *Surface and Coatings Technology, 93*(2–3), 158–167. https://doi.org/10.1016/S0257-8972(97)00037-6
196. Anders, A. (2002). From plasma immersion ion implantation to deposition: A historical perspective on principles and trends. *Surface and coatings technology, 156*(1–3), 3–12. https://doi.org/10.1016/S0257-8972(02)00066-X
197. Long, Z., Liu, K., Bai, B., & Yan, D. (2010). Corrosion resistance of modified layer on uranium formed by plasma immersion ion implantation. *Journal of alloys and compounds, 491*(1–2), 252–257. https://doi.org/10.1016/j.jallcom.2009.09.164
198. Kashkarov, E. B., Nikitenkov, N. N., Syrtanov, M. S., Sutygina, A. N., Shulepov, I. A., & Lider, A. M. (2016). Influence of plasma immersion titanium implantation on hydrogenation and mechanical properties of Zr–2.5 Nb. *Applied Surface Science, 370*, 142–148. https://doi.org/10.1016/j.apsusc.2016.02.149
199. Sutygina, A. N., Nikitenkov, N. N., Kashkarov, E. B., Syrtanov, M. S., Volesky, L., Louda, P., Priamushko, T. S., Sypchenko, V. S., & Hashhash, A. (2017). Influence of the plasma-immersion ion implantation of titanium on the structure, morphology, and composition of the surface layer of Zr–1Nb alloy. *Journal of Surface Investigation: X-ray, Synchrotron and Neutron Techniques, 11*(2), 452–457. https://doi.org/10.1134/S1027451017020343
200. Kashkarov, E., Nikitenkov, N., Sutygina, A., Laptev, R., Bordulev, Y., Obrosov, A., Liedke, M. O., Wagner, A., Zak, A., & Weiβ, S. (2018). Microstructure, defect structure and hydrogen trapping in zirconium alloy Zr-1Nb treated by plasma immersion

Ti ion implantation and deposition. *Journal of Alloys and Compounds, 732*, 80–87. https://doi.org/10.1016/j.jallcom.2017.10.151

201. Wang, S. Y., Chu, P. K., Tang, B. Y., Yan, J. C., & Zeng, X. C. (1998). Improvement of the wear and corrosion resistance of oil pump materials using plasma immersion ion implantation. *Surface and Coatings Technology, 98*(1–3), 897–900. https://doi.org/10.1016/S0257-8972(97)00173-4
202. Kurelo, B. C. S., de Oliveira, W. R., Serbena, F. C., & de Souza, G. B. (2018). Surface mechanics and wear resistance of supermartensitic stainless steel nitrided by plasma immersion ion implantation. *Surface and Coatings Technology, 353*, 199–209. https://doi.org/10.1016/j.surfcoat.2018.08.079
203. Li, T., Yuan, X., Li, R., Xiong, J., Tao, S., & Wu, K. (2021). Microstructure and Mechanical Characteristics of Dissimilar TIG Welded 9% Cr Heat-Resistant Steels Joints. *International Journal of Precision Engineering and Manufacturing, 22*, 1007–1019. https://doi.org/10.1007/s12541-021-00517-x
204. Han, C., & Doh, J. (2023). Investigation of fatigue characteristics for heat exchanger tube in air conditioner: effect of surface defect and environmental factor. *International Journal of Precision Engineering and Manufacturing, 24*, 867–875. https://doi.org/10.1007/s12541-023-00793-9
205. Mercan, S. (2021). Joining dissimilar material Pairs by mechanical locking method (MLM). *International Journal of Precision Engineering and Manufacturing, 22*, 1975–1987. https://doi.org/10.1007/s12541-021-00593-z
206. Kim, I. S., Lee, M. G., & Jeon, Y. (2023). Review on machine learning based welding quality improvement. *International Journal of Precision Engineering and Manufacturing Smart Technology, 1*, 219–226.
207. Laska, A., Szkodo, M., Pawłowski, Ł, & Gajowiec, G. (2022). Corrosion properties of dissimilar AA6082/AA6060 friction stir welded butt joints in different NaCl concentrations. *International Journal of Precision Engineering and Manufacturing-Green Technology*. https://doi.org/10.1007/s40684-022-00441-z
208. Basak, S., Mondal, M., Gao, K., Hong, S. T., Anaman, S. Y., & Cho, H. H. (2022). Friction stir butt-welding of roll cladded aluminum thin sheets: effect of microstructural and texture changes on mechanical properties. *Materials Science and Engineering: A, 832*, 142490. https://doi.org/10.1016/j.msea.2021.142490
209. Kwak, Y., Kang, T., Lee, S. H., & Kang, M. (2023). Effects of laser and tungsten arc welding processes on the thermal softening and mechanical properties of Almag6 aluminum alloy. *International Journal of Precision Engineering and Manufacturing, 24*, 531–536. https://doi.org/10.1007/s12541-023-00772-0
210. Kang, J. W., Zhnag, S., Bui Thi, T. A., Hong, S. T., Lee, S., & Hna, H. N. (2023). Friction-assisted dissimilar solid state lap joining of aluminum and copper pipes. *International Journal of Precision Engineering and Manufacturing, 24*, 199–208. https://doi.org/10.1007/s12541-022-00745-9
211. Mondal, M., Basak, S., Das, H., Hong, S. T., Choi, H., Park, J. W., & Han, H. N. (2021). Manufacturing of magnesium/aluminum bimetallic ring components by friction stir assisted simultaneous forging and solid-state joining. *International Journal of Precision Engineering and Manufacturing-Green Technology, 8*(5), 1429–1438. https://doi.org/10.1007/s40684-020-00244-0
212. Gao, K., Zhang, S., Mondal, M., Basak, S., Hong, S. T., & Shim, H. (2021). Friction stir spot butt welding of dissimilar S45C steel and 6061–T6 aluminum alloy. *Metals, 11*(8), 1252. https://doi.org/10.3390/met11081252
213. Mishra, R. S., & Ma, Z. Y. (2005). Friction stir welding and processing. *Materials Science and Engineering: R: Reports, 50*(1–2), 1–78. https://doi.org/10.1016/j.mser.2005.07.001
214. Gao, K., Basak, S., Mondal, M., Zhang, S., Hong, S. T., Boakye, S. Y., & Cho, H. H. (2022). Friction stir welding of AA3003-clad AA6013 thin sheets: Microstructural changes related to tensile properties and fatigue failure mechanism. *Journal of Material Research and Technology, 17*, 3221–3233. https://doi.org/10.1016/j.jmrt.2022.02.073
215. Hammood, A. S., Esmailzadeh, M., Hosseini, S. N., Karimi, S., Calliari, I., Pezzato, L., & Brittain, R. (2022). Effect of friction stir welding parameters on microstructure and corrosion behavior of 2101 duplex stainless steel in simulated body fluid. *International Journal of Precision Engineering and Manufacturing-Green Technology*. https://doi.org/10.1007/s40684-022-00440-0
216. Gao, K., Basak, S., Zhang, S., Hong, S. T., Boakye, S. Y., & Cho, H. H. (2023). Effects of the microstructure on the fatigue fracture of friction stir lap welded Al-clad Al and Al-clad steel sheets. *Journal of Material Research and Technology, 17*, 3221–3233. https://doi.org/10.1016/j.jmrt.2022.12.103
217. Nguyen, T. A. N., Basak, S., Zhang, S., Do, T. T., Mondal, M., Hong, S. T., Kim, M. J., & Han, H. N. (2022). Electrically assisted pressure joining of thin bi-layer aluminum-clad aluminum sheets. *International Journal of Advanced Manufacturing Technology, 121*, 4713–4723. https://doi.org/10.1007/s00170-022-09687-y
218. Kim, G. W., Song, K. H., & Jeong, S. M. (2022). Realization of enhanced mechanical properties of solid-state welded Ti alloy with commercial purity. *International Journal of Precision Engineering and Manufacturing, 23*, 471–477. https://doi.org/10.1007/s12541-022-00633-2
219. Lee, G., Kim, H., Jeon, J., Han, S., Han, S. W., & Cho, J. (2023). Development of plasma arc spot welding process and finite element method analysis model for predicting fracture strength: Part 1—development of plasma arc spot welding process. *International Journal of Precision Engineering and Manufacturing, 24*, 1–11. https://doi.org/10.1007/s12541-022-00707-1
220. Wang, J., Zhou, D., Xie, L., Li, X., Lu, Y., Bai, Z., & Zhou, J. (2021). Effect of multi-pass friction stir processing on microstructures and mechanical behaviors of as-cast 2A14 aluminum alloy. *Journal of Materials Engineering and Performance, 30*, 3033–3043. https://doi.org/10.1007/s11665-021-05594-7
221. Karthikeyan, L., Senthilkumar, V. S., Balasubramanian, V., & Natarajan, S. (2009). Mechanical property and microstructural changes during friction stir processing of cast aluminum 2285 alloy. *Materials & Design, 30*(6), 2237–2242. https://doi.org/10.1016/j.matdes.2008.09.006
222. Sutton, B., Ross, K., Grant, G., Cannell, G., Frederick, G., & Couch, R. (2017). Friction stir processing of degraded austenitic stainless steel nuclear fuel dry cask storage system canisters. In X. Liu, Z. Liu, K. Brinkman, S. Das, S. Dryepondt, J. W. Fergus, Z. Guo, M. Han, J. A. Hawk, T. Horita, P. Hosemann, J. Li, E. Olivetti, A. Pandey, R. B. Rebak, I. Roy, C. Shang, & J. Zhang (Eds.), Energy Materials 2017 (1st ed., pp. 343–351). Springer. https://doi.org/10.1007/978-3-319-52333-0_31.

**Sutanuka Mohanty** Project Associate in the School of Minerals, Metallurgical and Materials Engineering, Indian Institute of Technology Bhubaneswar, Odisha. She completed her Ph.D. in the department of Materials Science & Engineering from IIT Kanpur in 2016 and received her M.Tech. degree in Solid State Technology by the Department of Physics and Meteorology from the Indian Institute of Technology Kharagpur in 2011. She completed her M.Sc. in Physics from Utkal University, Bhubaneswar in 2008. She worked as Research Associate in the department of Physics at Indian Institute of Technology Guwahati, Assam from 2016 to 2018. Her current research interests include synthesis of High Entropy Alloys using mechanical alloying followed by consolidation using novel spark plasma sintering technique, their characterization, and applications in various fields. She has five international journal publications and few conference presentations to her credit.

**Soumyabrata Basak** obtained his Ph.D. in the School of Mechanical Engineering, University of Ulsan, Republic of Korea. His research interests include solid-state joining (FSW) and surface engineering of metallic materials.

**Debasis Saran** Ph.D. candidate at IIT Bhubaneswar in Material Science & Engineering. Prior to this, he was working as an Assistant Professor at SOA University, Bhubaneswar. He completed his M.Tech in 2016 from School of Minerals, Metallurgical & Materials Engineering, IIT Bhubaneswar. His research area includes conversion coatings, thermochemical hydrogen generation, magnesium alloys and corrosion. He is the recipient of the prestigious PMRF scholarship.

**Kajari Chatterjee** currently working as Institute Post-Doctoral Fellow in the School of Minerals, Metallurgical and Materials Engineering, IIT Bhubaneswar, Odisha. She received her Ph.D. from the same department in 2020. Before joining to IIT Bhubaneswar, she worked as Senior Scientific Officer at Indian Rubber Manufacturers Research Association (Affiliated to DPIIT, Ministry of Commerce & Industry, Govt of India), Mumbai from May 2007 to April 2008. She did her M.Tech. in Rubber Technology from IIT Kharagpur in 2007 and M.Sc. (Chemistry) from Kanpur University in 2003. Her current research interests include synthesis of Task specific room temperature ionic liquids and their applications in various fields especially in energy storage devices and metal extractions. She has several international journal and conference publications to her credit.

**Turin Datta** Ph.D. candidate in the School of Nanoscience and Technology at IIT Kharagpur. His research interests include bulk nanostructured alloys for structural applications, multi-component metallic alloys, surface degradation of structural materials, advanced surface engineering techniques and additive manufacturing of materials.

**Atul Kumar** currently working as Project Assistant in the School of Minerals, Metallurgical and Materials Engineering, IIT Bhubaneswar. He completed his M.Tech degree in Metallurgical and Materials Engineering in 2021 from IIT Bhubaneswar. His research interest area includes conversion coating, corrosion, magnesium alloys and duplex steels.

**Chandra Prakash** currently pursuing M.Tech in the School of Minerals, Metallurgical and Materials Engineering at Indian Institute of Technology, Bhubaneswar (IITBBS). His current research interests includes coating development and magnesium alloys.

**Doo-Man Chun** professor in the School of Mechanical Engineering at the University of Ulsan, South Korea. His research interests include fabrication of functional surfaces and hybrid manufacturing.

**Sung-Tae Hong** professor in the School of Mechanical Engineering at the University of Ulsan, South Korea. His research interests include metal forming, electrically assisted manufacturing, and solid state joining.

**Kisor Kumar Sahu** assistant professor in the School of Minerals, Metallurgical and Materials Engineering at Indian Institute of Technology, Bhubaneswar since 2012. He is a faculty member of Virtual and Augmented Reality Centre of Excellence (VARCOE) and Centre of Excellence for Novel Energy Materials (CENEMA), Indian Institute of Technology, Bhubaneswar. He is an editorial board member of "Scientific Reports", Nature Publications and Lead Guest Editor of "Materials for Nuclear and Fossil Energy Applications", Hindawi Publications. His current research interests include modelling & simulation, structural & magnetic frustration of materials, synchrotron and neutron diffraction, 3-D atom probe (LEAP), metallic glasses, process modelling, etc.